Progress in Oceanography 148 (2016) 56–73

Contents lists available at ScienceDirect

Progress in Oceanography

journal homepage: www.elsevier.com/locate/pocean

Uncertainty in climate projections for the 21st century northwest European shelf seas

Jonathan Tinker [a,*], Jason Lowe [a], Anne Pardaens [a], Jason Holt [b], Rosa Barciela [a]

[a] Met Office Hadley Centre, FitzRoy Rd, Exeter, Devon EX1 3PB, UK
[b] National Oceanography Centre, Joseph Proudman Building, 6 Brownlow Street, Liverpool L3 5DA, UK

ARTICLE INFO

Article history:
Received 18 March 2014
Received in revised form 2 August 2016
Accepted 5 September 2016
Available online 14 September 2016

ABSTRACT

There are a number of sources of uncertainty that impact climate projections for regional seas. We have assessed the impact that uncertain large-scale climate forcings have on the projections for the north-west European shelf seas. An ensemble of global Atmosphere-Ocean climate model (GCM) projections made by perturbed (atmospheric) parameter model variants which were designed to span uncertainty in climate sensitivity, was dynamically downscaled with the shelf seas model POLCOMS. The simulations were run as transient experiments (from 1952 to 2098) under a medium emissions scenario (SRES A1B). This study has focused on centennial changes over the period 2069–2098 relative to 1960–1989, but also refers to the full transient simulation to assess the significance of projected changes given interannual and low-frequency variability. The ensemble mean of the POLCOMS projections showed a shelf and annual mean Sea Surface Temperature (SST) rise of 2.90 °C ($\pm 2\sigma$ = 0.82 °C), and a Sea Surface Salinity (SSS) freshening of −0.41 psu ($\pm 2\sigma$ = 0.47 psu) between these periods. We described the spread in a field for a particular period using the variances associated with both the time mean ensemble dispersion (ensemble variance) and with the interannual variability. For SST in the present-day period, the magnitudes of both ensemble and interannual variance were fairly spatially homogenous. While the future interannual variance is of similar magnitude to that of the present day, the ensemble variance increased considerably into the future period. For SSS, both sources of variance were more spatially heterogeneous, and both increased into the future period. We investigated relationships between the projected shelf seas changes across the ensemble and changes in the large-scale climate forcing. We found that the near surface-air temperature from the driving GCM (averaged over the domain) and the GCM surface salinity to the west of the POLCOMS domain are good proxies for the changes within the shelf seas. We then compared these GCM indicators of shelf changes in our ensemble (under A1B) to the same measures across a number of CMIP5 models, under the RCP6.0 and RCP8.5 scenarios. The spread of these indicators, for our ensemble, fall within the range of the CMIP5 models (particularly under RCP8.5), suggesting our shelf projections would be consistent with an ensemble of projections driven by CMIP5 models.

1. Introduction

The North-West European (NWE) shelf seas are economically, environmentally and culturally important. They face many anthropogenic pressures ranging from overfishing, pollution to mineral extraction. However, they are particularly vulnerable to climate change (Holt et al., 2010). Many impacts of climate change and variability have already been observed on the NWE shelf ranging from significant temperature increases (Dye et al., 2013) to large northward species movement (e.g. Beaugrand et al., 2002). Currently there is a knowledge gap in estimates of the range of projected future changes in the shelf seas around the UK (e.g. MCCIP, 2012; Pinnegar et al., 2012).

In order to estimate the range of future plausible shelf sea changes, several types of uncertainty in large scale forcing climate need to be quantified, including from: model structure uncertainty, which arises from differences such as model resolution; model parameter uncertainty, which relates to uncertainty in parameters describing sub-grid-scale physical processes; forcing scenario uncertainty which accounts for uncertainty in future concentrations of greenhouse gases and other radiatively active constituents. Here we look at model parameter uncertainty using a Perturbed Physics Ensemble (PPE) of 11 Atmosphere-Ocean General Circulation Models (GCM) projections. GCMs are able to represent many

* Corresponding author.
E-mail address: jonathan.tinker@metoffice.gov.uk (J. Tinker).

http://dx.doi.org/10.1016/j.pocean.2016.09.003
0079-6611/

physical processes that drive large-scale climate change, but they are limited in their ability to properly simulate shelf seas. Firstly, GCMs are typically of too coarse a horizontal and vertical resolution to sufficiently capture the shelf sea regional topography. Secondly, they often exclude important shelf seas processes, such as tides. A common solution to providing shelf sea projections is to dynamically downscale a GCM projection by using its outputs to drive a regional shelf seas model. Here we downscale a set of 11 GCMs, with 11 Regional Climate Models (RCM) (each one is consistent with its parent GCM). The ocean component of the GCM and the surface component of the RCM are used to provide the ocean and atmosphere boundary conditions for the shelf sea model. Additionally riverine input is produced by a river routing model driven by model outputs from the RCMs.

A number of studies have used a similar approach for projections of the NWE shelf seas (e.g. Meier, 2006; Ådlandsvik, 2008; Holt et al., 2010, 2012; Olbert et al., 2012; Mathis and Pohlmann, 2014). To date, however, studies of future climate change in the NWE shelf region have generally taken a time-slice deterministic approach (e.g. Meier, 2006; Ådlandsvik, 2008; Holt et al., 2010). The time-slice approach is useful when considering spatial patterns, which are often lost when analysing time-series. It has the disadvantage, however, that the presence of long-term (>a few decades) variability in the climate system can increase or decrease projected changes if a peak (or trough) in the variability aligns with a time slice, leading to over- or under-estimation of the time-mean climate change. Our shelf seas projections are developed from those of Holt et al. (2010), who used the same shelf seas model and atmospheric forcings. However, they ran a time slice projection driven by a single member of the same global climate model ensemble as used here. They also used a delta change approach, where they created the future ocean boundary forcings by adding a modelled temperature (and salinity) change profile to the simulated present day forcings.

Our methodology overcomes many limitations of previous studies. We run an ensemble of transient shelf seas simulations from 1952 to 2098 (with the first eight years as spin-up) to consider uncertainty in projections. In this paper we generally concentrate on the changes across two 30-year periods (the minimum length of time-slice we consider suitable), of 1960–1989 and 2069–2098, so as to assess changes in spatial patterns, but with refer to the full transient changes to assess whether our conclusions are broadly robust given low frequency variability.

We focus our study of uncertainty in NWE shelf seas projections on the response to uncertainty in driving climate, given by the underlying PPE. Our shelf sea projections are the most comprehensive assessment of uncertainty arising from driving large-scale changes in climate to date.

We explore how our spread in projected shelf seas changes relate to changes in the large-scale driving climate. For this we consider parameters such as Equilibrium Climate Sensitivity (ECS, the modelled global temperature increase associated with a doubling of CO_2) and change in global (and regional) mean temperature, precipitation-minus-evaporation and salinity. We also consider change in locally important climate indices such as the North Atlantic Oscillation (NAO) and properties of the European storm track. Following on from this analysis we consider how to select driving models for future projection ensembles in order to best span uncertainty in the shelf seas projections.

2. Methods

The details of our modelling system framework are described in the study of Tinker et al. (2015), which focuses on evaluation of the present-day period in this ensemble of simulations. The modelling system uses a shelf seas model (POLCOMS), to downscale an ensemble of GCM historical simulations and climate projections. Here, we give a brief overview of the model system.

The climate projections are made by variants of the coupled atmosphere-ocean model HadCM3 (Gordon et al., 2000; Pope et al., 2000) and its regional atmospheric equivalent, HadRM3 (Jones et al., 2004). These models are the basis of a Perturbed Physics Ensemble (PPE) developed for the Quantifying Uncertainty in Model Projections (QUMP) project (Collins et al., 2011a). The variants of HadCM3 were run with flux-adjustment so as to allow exploration of a wider range of parameter uncertainty whilst still maintaining realistic present-day simulations. Thirty atmospheric model parameters were perturbed (singly or in concert) across this ensemble, within expert recommended ranges. For the design of this PPE, first a wider ensemble of perturbed parameter simulations was run, consisting of several hundred atmosphere-with-slab-ocean versions of HadCM3 (HadSM3). The effect of the parameter perturbations were assessed in this wider ensemble, both in terms of model skill at simulating observations and in terms of the emergent key climate response parameter of ECS. A set of 16 parameter combinations that spanned the full atmosphere-slab-ocean ensemble range of uncertainty in ECS, whilst validating well, were then selected to be used with the fully coupled PPE. These 16 perturbed ensemble members, together with the standard HadCM3 "unperturbed" parameter settings, produced a 17-member PPE of global projections.

The European atmosphere of each global PPE projection was dynamically downscaled with a consistent variant of the regional climate model HadRM3, with equivalent parameter perturbations. Unfortunately, one HadRM3 parameter perturbation (common to 6 ensemble members) led to poor validation at the regional scale. These ensemble members were not included in the regional downscaled PPE. These six ensemble member were distributed through the range of ECS, and so their exclusion is not thought to introduce a systematic bias in the regional ensemble in terms of this important parameter. Our regional atmospheric PPE therefore consists of the unperturbed member (termed ens_00) and a further 10 perturbed ensemble members (which we term ens_xx where xx is a number from 01 to 10, Table 1), giving an 11-member PPE of forcing projections. The spread of this 11-member regional ensemble contains a substantial fraction of the uncertainty compared to a distribution based on the same 11-members statistically inflated to account for a wider range of uncertainty (including additional emulated PPE members, and aspects of CMIP3 models structural uncertainty; Sexton et al., 2010). However, we consider our projections to provided a minimum estimate of model parameter uncertainty.

These forcings were used to drive a shelf seas projection ensemble from 1952 to 2098, with the first eight years considered spin-up, using specified greenhouse gas concentrations for the historical period and for the future period under the SRES (Special Report on Emissions Scenarios Nakicenovic et al., 2000) A1B scenario. The POLCOMS (Proudman Oceanographic Laboratory Coastal Ocean Modelling System; Holt and James, 2001; Holt et al., 2001) shelf sea model was used with HadCM3 providing the oceanic lateral boundary conditions and HadRM3 providing the downscaled atmospheric surface forcings. The HadRM3 runoff (from precipitation minus evaporation and any change in soil moisture and snow cover) was passed through the river routing model TRIP (Total Runoff Integrating Pathways; Oki and Sud, 1998; Oki et al., 1999) which provided the riverine forcing for POLCOMS. The riverine forcings did not have an associated water temperature value, but assume the temperature of the ocean grid-boxes into which they flow. The Baltic Sea outflow was treated as a river, with a climatological, observations-based, seasonal cycle of volume flux, temperature and salinity. While this treatment of the Baltic exchange was

Table 1
Details of individual ensemble members, and ensemble statistics. Change in near-surface air temperature and precipitation are from the driving HadCM3 simulation from the QUMP ensemble between 1961–1990 and 2070–2099. Here we consider the Europe as being within the model domain (longitude within 18°W and 13°E and latitude within 43°N and 63.5°N), and the western approach being 40–10°W, 50–60°N. Change in shelf SST and SSS relate to the annual and shelf mean change between 1960–1989 and 2069–2098. A "mean present-day" circulation pattern was calculated by averaging the upper 200 m depth-integrated currents for all ensemble member for the present-day (1960–1989) and a "future high-ECS" circulation pattern was calculated from ens_08-ens_10 for 2069–2098. For each ensemble member, the future mean u and v currents (annual mean, depth integrated for the upper 200 m, for locations with depths less than 500 m) were then correlated against both the "mean present-day" and "future high-ECS" circulation pattern, and these correlations are presented in the final columns. The upper rows give the figures for the 11 ensemble members, with ensemble statistics based on these 11 numbers given in bold in the rows below.

Ensemble member	Climate sensitivity (°C)	Change in global mean, near surface air temperature (°C)	Change in European mean, near surface air temperature (°C)	% Change in European mean, P-Ev	Change in Western Approach SSS (psu)	Change in shelf SST (°C)	Change in shelf SSS (psu)	Change in djf NAO	Change in AMO	Change in AMOC	Change in storm-track strength (hPa)	Change in storm-track location (°)	Spat corr coeff: fut circ with 'mean present-day' pattern	Spat corr coeff: fut circ with 'future high ECS' pattern
ens_00	3.50	3.22	3.07	10.31	−0.94	2.50	−0.41	0.00	0.09	−2.47	−0.20	−4.34	70.99	60.92
ens_01	2.52	2.38	2.68	13.72	−0.41	2.19	−0.26	0.63	−0.15	−3.05	−0.03	−1.81	91.85	36.37
ens_02	2.70	2.67	2.92	11.94	−0.45	2.36	−0.37	−0.15	0.19	−3.11	−0.29	−3.28	65.10	62.95
ens_03	3.51	3.18	3.26	14.71	−0.46	2.88	−0.12	−0.10	0.22	−3.30	−0.04	−5.73	74.35	53.74
ens_04	3.85	3.47	3.31	10.71	−0.43	2.78	−0.06	−0.55	0.00	−3.01	−0.65	1.11	82.55	47.55
ens_05	3.54	3.11	3.42	15.01	−0.66	2.88	−0.37	0.28	0.13	−2.65	0.15	−4.94	73.53	59.28
ens_06	4.08	3.53	3.73	6.25	−0.95	3.11	−0.42	−0.18	0.06	−2.21	−0.31	−6.50	51.72	81.43
ens_07	4.88	3.82	3.97	10.46	−0.70	3.39	−0.36	−0.23	0.41	−3.00	−0.34	−7.28	43.88	85.70
ens_08	4.97	3.83	3.80	10.57	−1.11	3.21	−0.65	0.03	0.43	−2.30	0.13	0.44	27.62	98.09
ens_09	5.32	4.25	3.86	22.85	−1.23	3.40	−0.72	0.10	0.37	−3.13	0.10	0.70	22.28	99.55
ens_10	5.46	4.16	3.94	19.29	−1.35	3.23	−0.74	−0.24	0.12	−2.95	−0.32	−2.77	17.23	98.21
ens mean	**4.03**	**3.42**	**3.45**	**13.26**	**−0.79**	**2.90**	**−0.41**	**−0.04**	**0.17**	**−2.83**	**−0.16**	**−3.13**	**56.46**	**71.25**
ens max	**5.46**	**4.25**	**3.97**	**22.85**	**−0.41**	**3.40**	**−0.06**	**0.63**	**0.43**	**−2.21**	**0.15**	**1.11**	**91.85**	**99.55**
ens min	**2.52**	**2.38**	**2.68**	**6.25**	**−1.35**	**2.19**	**−0.74**	**−0.55**	**−0.15**	**−3.30**	**−0.65**	**−7.28**	**17.23**	**36.37**
ens range	**2.93**	**1.88**	**1.30**	**16.60**	**0.94**	**1.21**	**0.68**	**1.18**	**0.58**	**1.09**	**0.80**	**8.39**	**74.62**	**63.18**

somewhat simplistic, in the absence of a coupled North Sea-Baltic Sea model many studies have used this approach (e.g. Ådlandsvik, 2008; Holt et al., 2010; Mathis and Pohlmann, 2014). As our climatology was not adjusted with the changing climate, it may affect our projections in the vicinity of the Skagerrak/Kattegat and the Norwegian Trench (NT), via the Norwegian Coastal Current – (NCC) which are downstream of the outflow, however, we expect little effect on the wider shelf. Evidence of this is provided by Holt et al. (2010) and Mathis and Pohlmann (2014). Holt et al. (2010) use the same Baltic forcings as we have, and note that their use of a climatology is unlikely to significantly affect the results on the shelf, but will have an effect in the vicinity of the Norwegian Coast. Mathis and Pohlmann (2014) modified the observed Baltic/North Sea volume exchange with a hydrological model of the run-off in the Baltic catchment (the Baltic/North Sea exchange increased at a rate of 0.001 Sv (6%) per 100 yrs) but used a climatological salinity cycle – they estimated a change salinity of the Baltic outflow salinity of 1 psu would lead to a 0.15 psu change in the NCC, and 0.02 psu in the entire North Sea. The climate change signal and variability may therefore be imposed on the shelf seas though the atmosphere, ocean or riverine forcings, although not through the Baltic Sea forcings. Although our modelling system is not fully coupled (the components do not feedback on themselves or the wider climate), the chain of driving models provides a self consistent set of forcings.

The shelf sea model domain covers the region 43°N–63°33′20″N and 18°20′W–13°E (Fig. 1). The model has 32 terrain following s-levels and a horizontal resolution of 1/9° latitude by 1/6° longitude (~12 km). For our analysis, the domain is divided into a number of regions, following Holt et al. (2012) (Fig. 1). For analysis purposes we consider the "shelf" region (used in regional means) to include the northern, central and southern North Sea, the English Channel, the Irish and Celtic Seas and the Irish and Shetland shelf regions, but to exclude the NT, Skagerrak/Kattegat and Armorican Shelf.

2.1. Evaluation of present day simulation and model drift

The modelling system used for this study was thoroughly evaluated by Tinker et al. (2015); here we briefly summarise their conclusions. In addition to the 11-member ensemble of downscaled historical and projection shelf sea simulations, Tinker et al. (2015) used the same modelling system to dynamically downscale an ERA-40 reanalysis simulation, to give a further historical simulation with observationally-derived forcings to aid evaluation. They compared the modelling system present-day simulations to two observational datasets: the predominantly satellite-based OSTIA (Operational sea Surface Temperature and sea Ice Analysis) (Roberts-Jones et al., 2012); and the quality controlled *in-situ* temperature and salinity profile dataset EN3 (Ingleby and Huddleston, 2007). Furthermore, volume transport through a number of cross-sections was compared to estimates from the literature.

A fixed-greenhouse-gas concentration pre-industrial climate "control" simulation (146 years), run with the unperturbed PPE member, was also downscaled to the NWE shelf seas with POLCOMS in order to assess model drift, to allow significance testing and to enable an assessment of unforced climate variability. This shelf sea control simulation showed that the drift in shelf surface and bed temperature and salinity for this ensemble member is small and generally insignificant (Tinker et al., 2015). The modelled present-day spatial patterns of temperature and salinity were found to be fit for purpose. The area-mean Sea Surface Temperature (SST) and Near Bottom Temperature (NBT) of the time-mean climate were also generally assessed to be good and sufficient respectively. Tinker et al. (2015) noted that care should be taken when interpreting the absolute values of the modelled salinity output, but concluded that the model system was generally sufficient as the basis of projection of salinity change. Within the Skagerrak/Kattegat and NT, however, the modelled mean salinity was assessed to be poor. This was attributed to the treatment of the Baltic and both the absolute and projected change in salinity

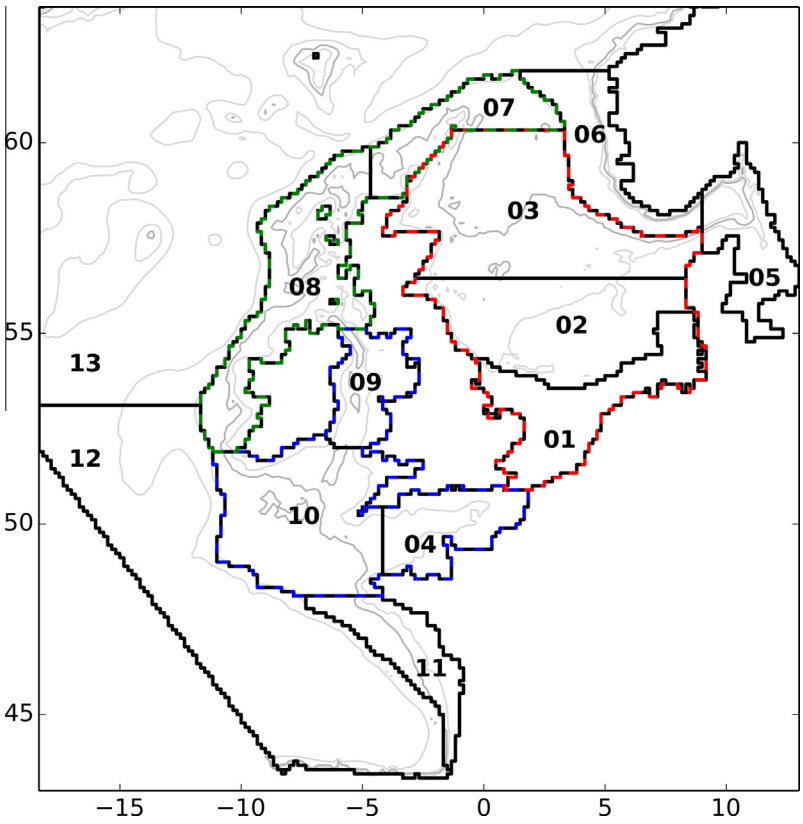

Fig. 1. Model domain and analysis regions: 01 Southern North Sea; 02 Central North Sea; 03 Northern North Sea; 04 English Channel; 05 Skagerrak/Kattegat; 06 Norwegian Trench; 07 Shetland Shelf; 08 Irish Shelf; 09 Irish Sea; 10 Celtic Sea; 11 Armorican Shelf; 12 NE Atlantic (S); 13 NE Atlantic (N); the shelf region is the southern, central and northern North Sea, the English Channel, the Shetland and Irish Shelf and the Irish and Celtic Seas.

(and of water column structure) are unlikely to be reliable in this region.

The biases of the shelf seas model, POLCOMS, have been extensively investigated in the context of operational oceanography (Holt et al., 2005). In addition, Holt et al. (2010) compared monthly-mean model fields from their present-day period simulation (using essentially the same POLCOMS configuration as considered here and forced by the same ens_00 atmospheric forcings) to gridded monthly mean observed data (their Section 3.3; Table 2) and found domain-wide mean and Root Mean Square (RMS) errors of: 0.5 °C and 1.4 °C for SST; 0.6 °C and 1.6 °C for NBT; −0.4 psu and 1.6 psu for Sea Surface Salinity (SSS); 0.2 psu and 1.5 psu for Near Bottom Salinity (NBS).

Table 2
Sources of climate projection uncertainty, and how they are addressed within this study.

Uncertainty source	Addressed
Model parameter uncertainty	Yes. Uncertainty in the GCM atmosphere parameters is explored. Parameters in other components of the GCM led to less uncertainty in the global temperature projections and so are excluded Uncertainty in the parameters of the shelf seas model is not explored
Emission scenario uncertainty	No. A single SRES emission scenario (A1B) is used
Model structure uncertainty	No. A single GCM (HadCM3) is downscaled with a single shelf seas model (POLCOMS)
Model driving methodology uncertainty	No. Uncertainty associated with the choice of forcing methodology (one-way forcing or two-way coupling with the local atmosphere or wider climate) is not explored

2.2. Sources of uncertainty in these climate projections

As we have noted, there are a number of sources of uncertainty that impact climate projections. Here we describe different aspects of climate projection uncertainty and their relationship to our study (summarised in Table 2). The "perturbed parameter" uncertainty, which we focus on here, arises due to the relatively coarse grid-size of climate models, which means that many important small-scale processes are not explicitly modelled. Such "sub-grid-scale" processes are parameterised by relating their behaviour to large-scale processes that are captured on the model grid. Such parameterisations, and the parameters within them, are often based around observations and laboratory experiments, and/or are adjusted to give an acceptable evaluation of the model. Due to measurement error, insufficient data, and lack of physical understanding, such parameterisations are a significant source of uncertainty in climate model projections. The QUMP project ran a number of PPEs to explore the uncertainty associated with such parameters within key Earth system component models, including the atmosphere, ocean, carbon cycle and sulphur cycle models. The global mean temperature response was most sensitive to atmosphere parameter perturbations, and so we have chosen to use this PPE for our study.

The PPE we have used as our forcing ensemble was designed to span the maximum range of ECS given by the possible perturbed parameter combinations, with the restriction of the present-day climate being reasonably simulated (in the slab models) compared to observations. This range of ECS is 2.52–5.46 °C (from the 11-member PPE, Table 1, Glen Harris Pers. Comm.) compared to the 2.1–4.7 °C (Andrews et al., 2012) in 5th phase of the Coupled Model Intercomparison Project (CMIP5) model projections for the IPCC Fifth Assessment (IPCC, 2013), under RCP6.0 (the closest CMIP5

scenario to A1B in terms of radiative forcing, Sexton et al., 2013). While the QUMP and CMIP5 spread in global temperature and percent precipitation change are similar (Table 3), within the European domain the QUMP spread is smaller (CMIP5: 2.19 °C (21.44%); QUMP: 1.38 °C (6.48%) for temperature (percent precipitation) change).

It should be noted that for the uncertainty in NWE shelf sea projections, the uncertainty in changes in key local climate fields is likely to be more critical than uncertainty in global climate. It was beyond the scope of this project, however, to design and generate a forcing ensemble to specifically focus on NWE shelf seas uncertainty. A key question for us, therefore, is whether the ECS turns out to be a good predictor of spread. We also note that we have not explicitly studied model structural uncertainty and shelf sea projections driven by downscaled versions of other GCMs may give different future results. One indicator of uncertainty in local NWE shelf seas climate is likely to be given by the behaviour of the European storm track. Projections of the European storm track (evaluated at 4°W longitude) in the QUMP PPE tend to produce a general weakening and a southward movement over the 21st century, whereas in the CMIP3 Multi-Model Ensemble (MME) there is less of a southward movement, and no clear change in strength (Lowe et al., 2009). CMIP5 storm activity projections in this region for the end of century are similar to those from CMIP3, but suggest a slight projected increase in activity over north-western Europe (e.g. Harvey et al., 2012).

There are currently newer climate models than HadCM3, around which our PPE is based, with more advanced physics (e.g. HadGEM3, Hewitt et al., 2011; Megann et al., 2014; Williams et al., 2015) or more earth system complexity (e.g. HadGEM2, Collins et al., 2011b). However, such models have not yet been used to generate PPEs and so are presently unsuitable for providing driving forcings for our purpose.

Finally, there are a range of methodologies that can be used to downscale GCM climate projections for shelf seas and this introduces another source of uncertainty. We have used a single one-way nested dynamic downscaling approach. Alternative methodologies include to use a two-way coupling between global and regional atmosphere-ocean models (e.g. Schrum et al., 2003), two-way coupling with the lateral ocean or a refined mesh to give higher resolution over the regional of interest (e.g. Gröger et al., 2013).

2.3. Describing the ensemble behaviour

As a simple measure of uncertainty we calculate the ensemble mean projection and its standard deviation using the unweighted 30-year means of the 11 ensemble members. We make the assumption of a Gaussian distribution (supported by the Shapiro-Wilk test at the 5% level, $n = 11$), under which ~95% of the ensemble members are expected to be within ±1.96 standard deviations of the ensemble mean. The distributions of projected surface warming (dSST) across the ensemble for two example regions, the southern North Sea, which is a permanently mixed inner shelf region and the Shetland Shelf, which is a seasonally stratified region strongly influenced by the oceanic conditions, qualitatively supports the assumption of normality (Fig. 2). When looking at dSSS (change in SSS), however, there is an apparent bifurcation in the ensemble, with ensemble members ens_08 – ens_10 behaving qualitatively differently. Although the distribution of dSSS is still statistically normal for all regions ($p > 0.05$, Shapiro-Wilk test), care must be taken when interpreting the ensemble mean salinity products.

For simplicity, we use two times the standard deviation (2σ) to describe the ensemble spread (average ± x, where $x = 2\sigma$). We calculate 2σ for each grid box, for a given month (and season and year) across each of the 30 year time periods, then report the area-average in each region (Table 4, these values are consistent with the values presented in the ensemble variance maps in Figs. 4–7). The typical interannual variability, however, is often greater than the ensemble time mean spread (see individual years shown in Fig. 2). A more sophisticated analysis of the ensemble variability is a decomposition of the total variance (σ^2_{tot}) into an interannual variability component (σ^2_{int}), which is the mean of the 30-year interannual variances for each ensemble member, and an ensemble spread component (σ^2_{ens}), which is the variance of the 30-year means for the ensemble:

$$\sigma^2_{\mathrm{int}} = \frac{\sum_{e,y}\left((x_{e,y})^2\right)}{n_e n_y} - \frac{\sum_e \left(\left(\frac{\sum_y x_{e,y}}{n_y} \right)^2 \right)}{n_e}$$

$$\sigma^2_{\mathrm{ens}} = \frac{\sum_e \left(\left(\frac{\sum_y x_{e,y}}{n_y} \right)^2 \right)}{n_e} - \left(\frac{\sum_{e,y} x_{e,y}}{n_e n_y} \right)^2$$

$$\sigma^2_{\mathrm{tot}} = \sigma^2_{\mathrm{int}} + \sigma^2_{\mathrm{ens}} = \frac{\sum_{e,y}\left((x_{e,y})^2\right)}{n_e n_y} - \left(\frac{\sum_{e,y} x_{e,y}}{n_e n_y} \right)^2$$

where this decomposition uses the sum of squares formula and where $x_{e,y}$ denotes a variable (such as SST) for a given year y, and ensemble member e, n_y is the number of years in the sample (30) and n_e the number of ensemble members (11).

These components of variance give a measure of how much the time mean year varies across the ensemble, and how it compares to the variance of individual years within the meaning period (shown for the two example areas in Fig. 2 and spatially

Table 3
Global and European mean temperature (°C) and precipitation (%) change (between 1961–1990 and 2070–2099), for the CMIP5 ensemble (under, RCP6.0, the closest CMIP5 scenario to A1B in terms of radiative forcing, Sexton et al., 2013) and the 11- and 17-member global QUMP PPE (under SRES A1B), for the ensemble mean, and the ensemble spread (ensemble max – ensemble mean). The CMIP5 models include: CCSM4, CESM1-CAM5, CSIRO-Mk3-6-0, FIO-ESM, GFDL-CM3, GFDL-ESM2G, GFDL-ESM2M, GISS-E2-H, GISS-E2-R, HadGEM2-AO, HadGEM2-ES, IPSL-CM5A-LR, IPSL-CM5A-MR, MIROC-ESM-CHEM, MIROC-ESM, MIROC5, MRI-CGCM3, NorESM1-ME, NorESM1-M, bcc-csm1-1-m, bcc-csm1-1. Here we consider the Europe as being within the model domain (longitude within 18°W and 13°E and latitude within 43°N and 63.5°N).

	Global Mean		European Mean	
	Ens Mean	Ens Spread (max–min)	Ens Mean	Ens Spread (max–min)
Near-Surface Air Temperature: change between 1961–1990 and 2070–2099 (°C)				
CMIP5 RCP6.0	2.499	1.659	2.39	2.194
QUMP-11	3.531	1.883	3.669	1.381
QUMP-17	3.418	1.984	3.601	1.648
Precipitation: change between 1961–1990 and 2070–2099 (%)				
CMIP5 RCP6.0	4.244	4.57	2.573	21.438
QUMP-11	4.952	4.579	3.388	6.475
QUMP-17	4.665	4.973	3.086	7.157

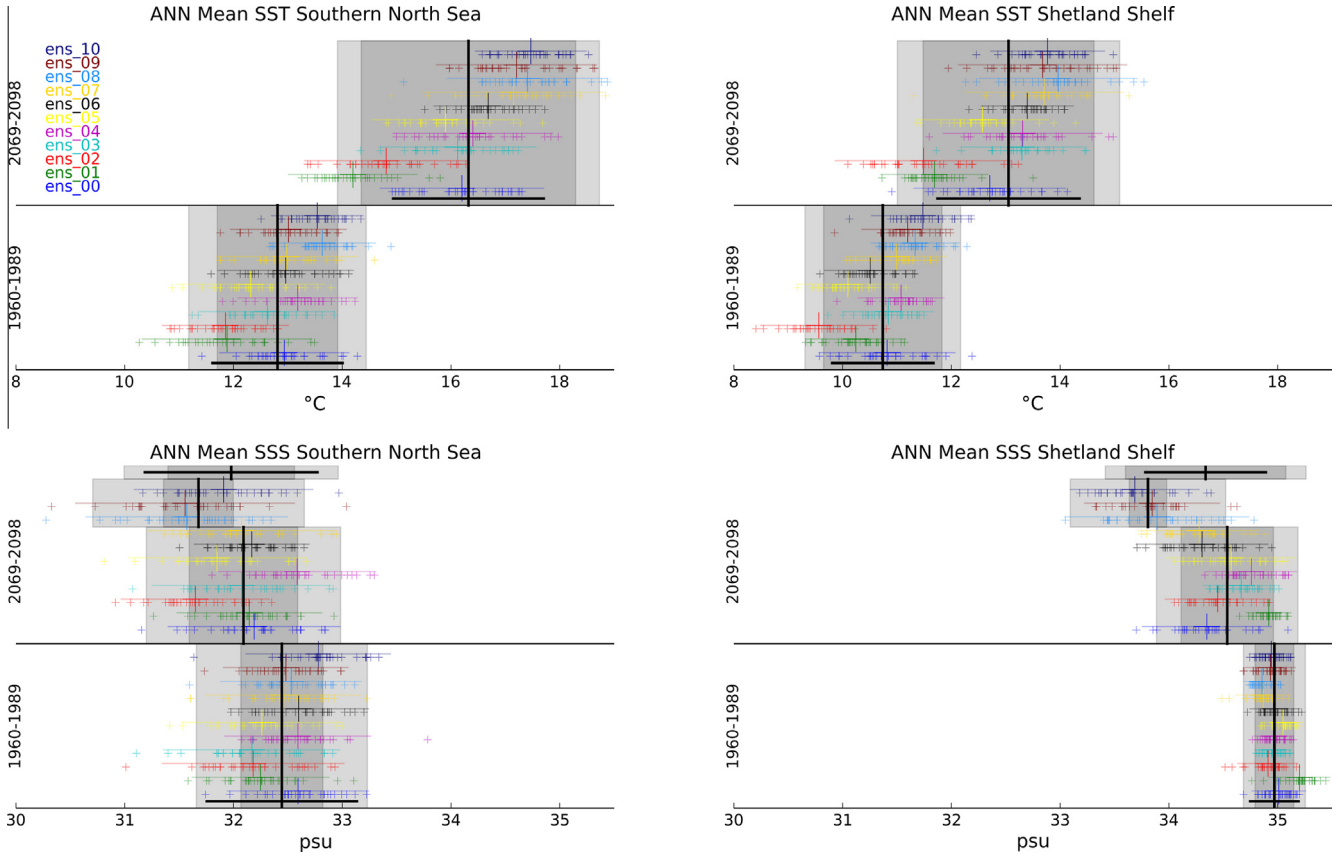

Fig. 2. Annual and area mean SST and SSS for two exemplar regions (southern North Sea and Shetland Shelf) and periods (present day 1960–1989 and future, 2069–2098) are presented to show the ensemble and inter-annual variability. Each ensemble member is represented by a different colour, with each small + representing a single annual mean value for that ensemble member. The 30-year mean and interannual variability for each ensemble member is shown with the coloured larger coloured vertical ticks and horizontal line ($\pm 2\sigma$). The vertical black lines represented the ensemble mean for each period. The light grey shading shows $\pm 2\sigma$ of the 330 annual means, and so represents the total (ensemble and interannual) variability. The dark grey shading shows the ensemble variability (ensemble mean $\pm 2\sigma$ from the 30 year means). The horizontal black line represents the ensemble mean $\pm 2\sigma$ as calculated from the interannual variance, to allow comparison between the ensemble variance (dark grey shading) and interannual variance (black horizontal line). Three ensemble members have future salinity distinct from the rest of the ensemble (ens_08–ens_10). This is illustrated by separating the ensemble into two parts. Here, the vertical bold line and shading are calculated for their respective sub-ensembles. Above the divided ensemble, the full ensemble mean, ensemble standard deviation and interannual variability is given (as calculated from all 11 members). Note that all variability is expressed as ±1.96 times the square-root of the variance, to give (±1.96 times) the standard deviation as calculated from the ensemble, interannual or total variance. This is done to include ~90% of the data (assuming normality), however this make it difficult to directly combine the ensemble and interannual variance to give the total variance, hence all three are included.

Table 4
End of century projected change (2069–2098 relative to 1960–1989) in annual mean SST, SSS, NBT, NBS and summer PEA, PEAT, PEAS and MLD for ensemble mean ($\pm 2\sigma$) averaged over shelf regions. 2σ is two times the ensemble standard deviation, which is the square root of the ensemble variance ($\sqrt{\sigma^2_{ens}}$). These are calculated by taking the regional means from the data used to produce the Figs. 4–7. Note that for vertically mixed regions the PEA is <10 J/m^3 (often ~ 0) whereas the Mixed Layer Depth is not calculated (left as NaN). This may affect the regional averages.

	Shelf	Southern North Sea	Central North Sea	Northern North Sea	English Channel	Irish Sea	Celtic Sea
Ann dSST (°C)	2.90 (±0.82)	3.26 (±0.72)	3.15 (±0.75)	2.75 (±0.75)	3.13 (±0.82)	3.08 (±0.85)	3.01 (±1.04)
Ann dSSS (psu)	−0.41 (±0.47)	−0.51 (±0.61)	−0.48 (±0.53)	−0.62 (±0.65)	−0.08 (±0.25)	−0.18 (±0.27)	−0.11 (±0.23)
Ann dNBT (°C)	2.71 (±0.75)	3.22 (±0.71)	2.92 (±0.63)	2.53 (±0.63)	3.04 (±0.79)	3.00 (±0.82)	2.54 (±0.88)
Ann dNBS (psu)	−0.33 (±0.38)	−0.49 (±0.58)	−0.47 (±0.48)	−0.52 (±0.52)	−0.08 (±0.24)	−0.18 (±0.26)	−0.03 (±0.19)
Ann dDFT (°C)	0.19 (±0.24)	0.05 (±0.04)	0.24 (±0.29)	0.22 (±0.31)	0.09 (±0.05)	0.08 (±0.06)	0.47 (±0.32)
Ann dDFS (psu)	−0.08 (±0.12)	−0.02 (±0.05)	−0.01 (±0.08)	−0.09 (±0.15)	−0.00 (±0.01)	−0.01 (±0.01)	−0.08 (±0.11)
Sum dMLD (m)	0.86 (±1.01)	0.15 (±0.93)	0.23 (±0.83)	0.66 (±1.08)	0.80 (±0.76)	1.68 (±1.35)	0.96 (±0.75)
Sum dPEA (J/m^3)	18.55 (±13.95)	1.55 (±2.11)	12.86 (±10.82)	22.52 (±18.96)	3.43 (±1.99)	3.75 (±2.25)	31.90 (±18.15)
Sum dPEAT (J/m^3)	10.87 (±7.04)	0.85 (±0.77)	12.42 (±6.95)	13.97 (±8.30)	3.48 (±1.74)	3.89 (±2.03)	24.11 (±11.91)
Sum dPEAS (J/m^3)	7.68 (±11.10)	0.70 (±1.57)	0.44 (±5.33)	8.56 (±14.68)	−0.06 (±0.50)	−0.14 (±0.72)	7.80 (±11.06)

in Figs. 4–7). The values are then averaged over sub-regions (as mapped in Fig. 1) and tabulated (Tables 4 and 5).

There are two ways of giving the variance for a region: calculating the regional mean values for each year, and then calculating the variance from these; or calculating the variance for each grid-box and then reporting the regional mean of these. We report the latter, as the values are then easier to interpret with the spatial variance maps (Figs. 4–7). However, there is a risk that a feature moving within a region between different ensemble members may dominate these variances: a large magnitude ensemble variance, for example, would then not reflect variance across the ensemble of the regional mean. In order to assess whether this is the case, we

Table 5
End of century projected change (2069–2098 relative to 1960–1989) in annual mean SST, SSS, NBT, NBS and summer PEA, PEAT, PEAS and MLD for ensemble variance (σ^2_{ens}) and interannual variability (σ^2_{int}) averaged over shelf regions. These are calculated by taking the regional means from the data used to produce the figures. Note that for mixed regions the PEA is <10 J/m^3 (often ~ 0.) whereas the Mixed Layer Depth is not calculated (left as NaN). This may affect the regional averages. (σ^2_{ens}; σ^2_{int}).

	Shelf	Southern North Sea	Central North Sea	Northern North Sea	English Channel	Irish Sea	Celtic Sea
Ann dSST var (°C^2)	0.45; 0.08	0.42; 0.05	0.44; 0.07	0.40; 0.09	0.47; 0.04	0.48; 0.06	0.59; 0.07
Ann dSSS var (psu^2)	0.06; 0.04	0.06; 0.02	0.05; 0.04	0.13; 0.06	0.01; 0.01	0.01; 0.02	0.01; 0.02
Ann dNBT var (°C^2)	0.34; 0.06	0.40; 0.06	0.27; 0.08	0.26; 0.09	0.42; 0.04	0.43; 0.05	0.34; 0.03
Ann dNBS var (psu^2)	0.04; 0.03	0.06; 0.03	0.05; 0.04	0.08; 0.04	0.00; 0.01	0.01; 0.01	−0.00; 0.01
Ann dDFT var (°C^2)	0.02; 0.03	0.00; 0.01	0.03; 0.03	0.04; 0.03	0.01; 0.00	0.00; 0.00	0.04; 0.02
Ann dDFS var (psu^2)	0.01; 0.01	0.00; −0.00	−0.00; 0.00	0.01; 0.01	0.00; 0.00	0.00; 0.00	0.01; 0.01
Sum dMLD var (m^2)	0.26; −0.42	−0.03; −0.64	0.16; −0.26	0.41; −0.34	−0.16; −0.81	−0.28; −3.99	0.08; −0.21
Sum dPEA var (J^2/m^6)	161.86; 113.91	4.93; 12.92	40.01; 60.59	191.50; 162.53	8.87; 2.85	8.17; 5.78	231.68; 106.10
Sum dPEAT var (J^2/m^6)	28.90; 34.67	0.59; 3.18	28.17; 24.48	41.60; 35.43	8.12; 2.63	6.33; 7.59	79.03; 57.53
Sum dPEAS var (J^2/m^6)	101.33; 132.10	3.58; 5.09	2.79; 19.72	104.77; 136.55	0.18; 0.89	0.49; 1.42	76.32; 127.84

have examined how the spatial cumulative distribution frequencies change between the present day and the future period, together with the spatial correlation of the fields (for example SST) between the two periods (not shown), for each ensemble member. Due to the very high spatial correlations (>95%) and the general offset between the CDFs with little change in shape, we infer that the change in variance for a region generally reflects the spread in regional area-averages.

The ensemble variance may potentially be suppressed in the present day by the flux adjustment approach used in the QUMP PPE. As we have noted, additional heat and freshwater flux "adjustments" are applied to each QUMP ensemble member; these prevent the present-day simulation deviating too far from observed climatology and correspondingly remove the same bias from the future period. These adjustments were calculated from earlier model runs, which were relaxed to observation-derived SST climatology fields with timescales of 30 days for temperature and 120 day for salinity (Collins et al., 2011a). For this reason comparisons between present day ensemble and interannual variance must be treated with care. The ocean acts as a time-integrator of imbalances between surface and ocean boundary fluxes for a water column; as such ensemble spread will tend to increase with time.

2.4. Describing the water column structure

The NWE shelf seas contain regions that seasonally stratify (e.g. the northern North Sea) and regions that are permanently mixed (e.g. the southern North Sea) separated by tidal mixing fronts (Simpson and Bowers, 1981). While the dominant mechanisms that lead to the locations of these fronts are not primarily affected by climate change (but rather by tides and bathymetry), the strength and depth of the pycnocline in the stratified regions are. Here we consider the Potential Energy Anomaly (PEA; Simpson and Bowers, 1981) as a measure of the strength of the stratification – here we take PEA >10 J/m^3 to denote that the water column is stratified. The PEA can be separated into temperature and salinity components (PEAT and PEAS respectively). We also use the Mixed Layer Depth (MLD) (Wakelin et al., 2009) to describe the vertical structure of a stratified water column. Both PEA and MLD are described in detail by Tinker et al. (2015).

The MLD and PEA are two aspects of stratification which are related but can be controlled by different processes. The MLD is the depth of the upper part of the water column that is well mixed and can change with changing wind forcing. While the MLD will feed into the PEA, the PEA reflects the strength of the stratification over the entire water column. As an illustration: PEA can be increased by an increasing seasonal cycle of SST as the NBT tends to remain similar to the winter SST (when the water column is fully mixed); this would not necessarily affect MLD.

3. Projected changes in shelf sea fields

Here we describe the projected changes in shelf sea fields, and their uncertainty. We first give an overview of the projected changes to the circulation pattern, which can help put the temperature and salinity changes (which we describe later) into context. We also describe changes in water column structure. We describe the ensemble mean change, and consider the ensemble and interannual variance.

3.1. Circulation

The overall circulation of the NWE shelf seas plays an important role in the distribution of ocean quantities, particularly of salinity and other similarly more "passive" quantities (in the sense of being less subject to damping by surface fluxes). In addition to possible changes in the strength of the currents, their spatial pattern (configuration) is also subject to change.

The present day time-mean circulation configuration (Fig. 3; evaluated as depth average of the upper 200 m) is fairly consistent across the ensemble (visually, and quantitatively in terms of the spatial vector correlation (Crosby et al., 1993) which considers both magnitude and direction of the vector field). This is supported by the similarity across the ensemble of the volume transport cross-sections calculated by Tinker et al. (2015) (their Fig. 10). The shelf break current is the most prominent shelf-wide circulation. Holt et al. (2010) found a substantial decrease in the future period shelf break current at 56°N (~1 Sv: Lowe et al., 2009); here we also find an ensemble mean reduction, of 1.24 Sv, but there is considerable ensemble spread ($\pm 2\sigma$ = 1.53 Sv).

Into the future there is an apparent divergence in the configuration of the time-mean circulation across the ensemble: some ensemble members (ens_08-ens_10) have areas of considerable change, other members (ens_01-ens_05) tend to change little from their present day configuration and the rest are between these two states. The greatest changes in the circulation configuration patterns are for the highest ECS ensemble members (ens_08-10). We average the circulation pattern of the present day for all ensemble members to produce a 'mean present-day' circulation pattern, and then average the future circulation patterns of the highest ECS ensemble member to produce a 'future high-ECS' pattern (Fig. 3). We then correlate the present day and future circulation pattern of each ensemble member against these patterns (using the spatial vector correlation (Crosby et al., 1993)). In the present day all ensemble members have high spatial vector correlations with the 'mean present-day' pattern and low correlations with the 'future high-ECS' pattern. In the future period, the spatial vector correlation between each ensemble member and the 'future high-ECS' ('mean present-day') pattern itself correlates positively (negatively) with ECS (Tables 1 and 6).

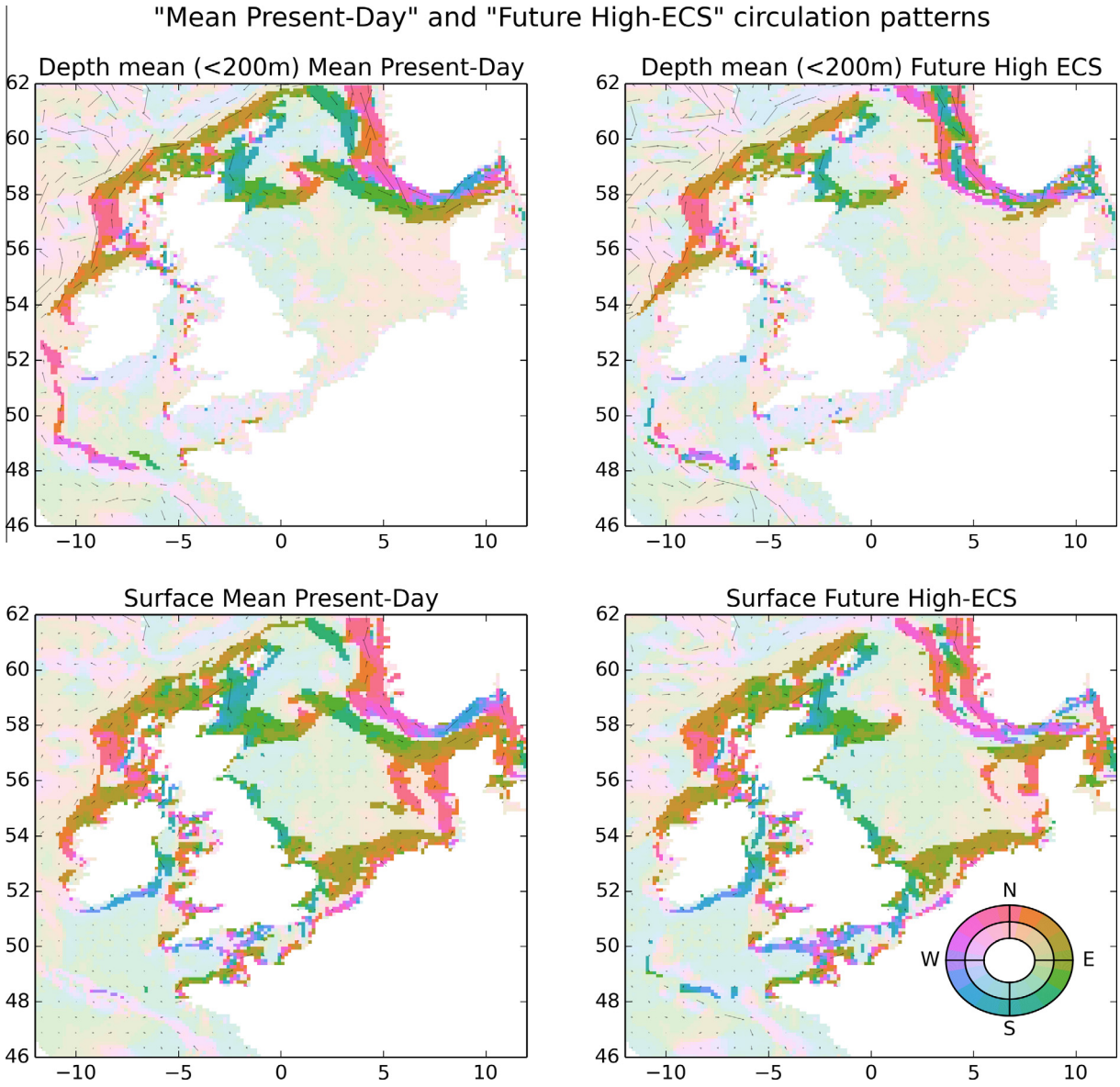

Fig. 3. 'Mean present-day' (1960–1989) and 'future high-ECS' (2070–2098, ens_08-ens_10) circulation configuration, for the 30-year, annual depth-mean (of the upper 200 m, upper row) and surface currents (lower row). The vectors represent the direction and magnitudes. The colouring highlights the direction of the currents (directions that the currents are going to) on the shelf (<500 m) when the magnitude exceeds a threshold of 4 m^2/s. Below this threshold and in regions with depths greater than 500 m, the colouring and vectors are much lighter.

Table 6
The correlation between the ECS/shelf response from the 11 ensemble member with the 11 associated driving data summary statistics/climate indices. ECS: Climate sensitivity, dSST/dSSS change in SST and SSS averaged over the shelf; dCircP: Spatial vector correlation coefficient of future circulation with "Mean Present-Day" mean circulation pattern; dCircF: Spatial vector correlation coefficient of future circulation with "Future High-ECS" mean circulation pattern. We note that a sample size of 11 is small, and that the absolute Pearson's correlation coefficients greater than 0.623 are significant at the 5% level assuming a two-tailed test – insignificant correlations are greyed out.

	ECS	dSST	dSSS	dCircP	dCircF
ECS (°C)	1.000	0.929	−0.698	−0.903	0.896
Change in global mean, near surface air temperature (°C)	0.983	0.923	−0.639	−0.864	0.865
Change in European mean, near surface air temperature (°C)	0.956	0.949	−0.624	−0.882	0.898
% Change in European mean, P-Ev	0.369	0.258	−0.459	−0.394	0.280
Change in European SSS (psu)	−0.673	−0.491	0.985	0.848	−0.813
Change in Western Approach SSS (psu)	−0.820	−0.659	0.919	0.881	−0.872
Change in djf NAO	−0.359	−0.364	−0.129	0.234	−0.250
Change in AMO	0.639	0.716	−0.465	−0.685	0.728
Change in AMOC	0.142	0.142	−0.307	−0.171	0.281
Change in storm-track strength (hPa)	0.036	0.095	−0.387	−0.164	0.171
Change in storm-track location (°)	0.184	−0.032	−0.226	−0.157	0.082
ECS (°C)	1.000	0.929	−0.698	−0.903	0.896
dSST (°C)	0.929	1.000	−0.538	−0.810	0.841
dSSS (psu)	−0.698	−0.538	1.000	0.885	−0.863
dCircP: Spatial vector correlation coefficient of future circulation with "Mean Present-Day" mean circulation pattern	−0.903	−0.810	0.885	1.000	−0.986
dCircF: Spatial vector correlation coefficient of future circulation with "Future High-ECS" mean circulation pattern	0.896	0.841	−0.863	−0.986	1.000

The greatest changes in shelf circulation configuration, as evident for the high ECS ensemble members, tend to occur in the northern part of the North Sea (Fig. 3). In the time-mean present day configuration, the Dooley current (an eastward North Sea current that flows from the Scottish coast at ~58°N and across the North Sea) feeds into a south-eastwards current, adjacent (but opposite in direction) to the Norwegian Coastal Current (NCC). It retroflects within the Skagerrak, and then feeds into the NCC. Along the northern edge of the North Sea is the shelf break current, which in the present day follows the shelf break eastwards before turning southeast into the NT. In the future high ECS ensemble members, the Dooley current weakens (Fig. 3) and rather than extending into a south-eastward current adjacent to NCC, there is instead a northwestward current parallel to the NCC, leaving the shelf. The shelf break current north of Scotland weakens, and no longer flows into the NT. These changes mean that water in the eastern North Sea often has a different providence in the future high ECS ensemble members: for example, the western NT has water originating in the North Atlantic in the present day but may have water coming from the Skagerrak in the future period; this has important implications, particularly for future salinity in this region. These changes are apparent in both the upper 200 m depth averaged currents and the surface currents (Fig. 3).

3.2. Temperature

There is a substantial increase in SST across the shelf between the present day (1960–1989) and the future period (2069–2098), with an annual and ensemble mean rise in SST (averaged across the shelf) of 2.90 °C ($\pm 2\sigma = 0.82$ °C). There is a spatial pattern to the warming which varies seasonally, with greatest winter/spring warming in the south-east North Sea, and greatest summer/autumn warming in the Celtic Sea and North Sea (see Fig. 4, Table 4 for regional values). Future interannual variability in SST is similar to that of present day in both magnitude and pattern. Interannual variability in the shallow southern North Sea, German Bight, and Skagerrak/Kattegat has seasonal maxima in winter, but otherwise interannual variability is fairly similar across the domain and seasons (Fig. 4). SST ensemble variance increases between the present day and the future period, particularly in the summer and autumn. The shelf and annual mean future ensemble variance is greater than the interannual variance. In the winter, the NBT across the shelf warms at a similar rate as SST. In the summer, the SST in the stratified regions tends to increase more than the NBT, which tends to increase the surface minus bed temperature (DFT; Sup. Fig. 2) in these regions (also expressed by PEAT, see later).

3.3. Salinity

There is a general freshening across the shelf between the present day (1960–1989) and the future period (2069–2098), with an annual mean (averaged across the shelf) change in SSS of −0.41 psu ($\pm 2\sigma = 0.47$ psu) (Fig. 5, Table 4). There is more spatial heterogeneity in the shelf SSS pattern of change than for SST, reflecting the increased importance of advective processes and of local freshwater inputs. The shelf NBSs tend to reflect the (values and patterns of) SSS, with the exception of in the NT and locally at some river mouths (Sup. Fig. 1). The NT is strongly haline stratified due to the large input of freshwater from the Baltic outflow, with saline oceanic water inflowing beneath.

In the present day period, the salinity boundary forcings are fairly constant with depth and location and also across the ensemble, (present day ensemble and annual mean salinity forcing averaged around the boundary at all depths is 35.11 psu

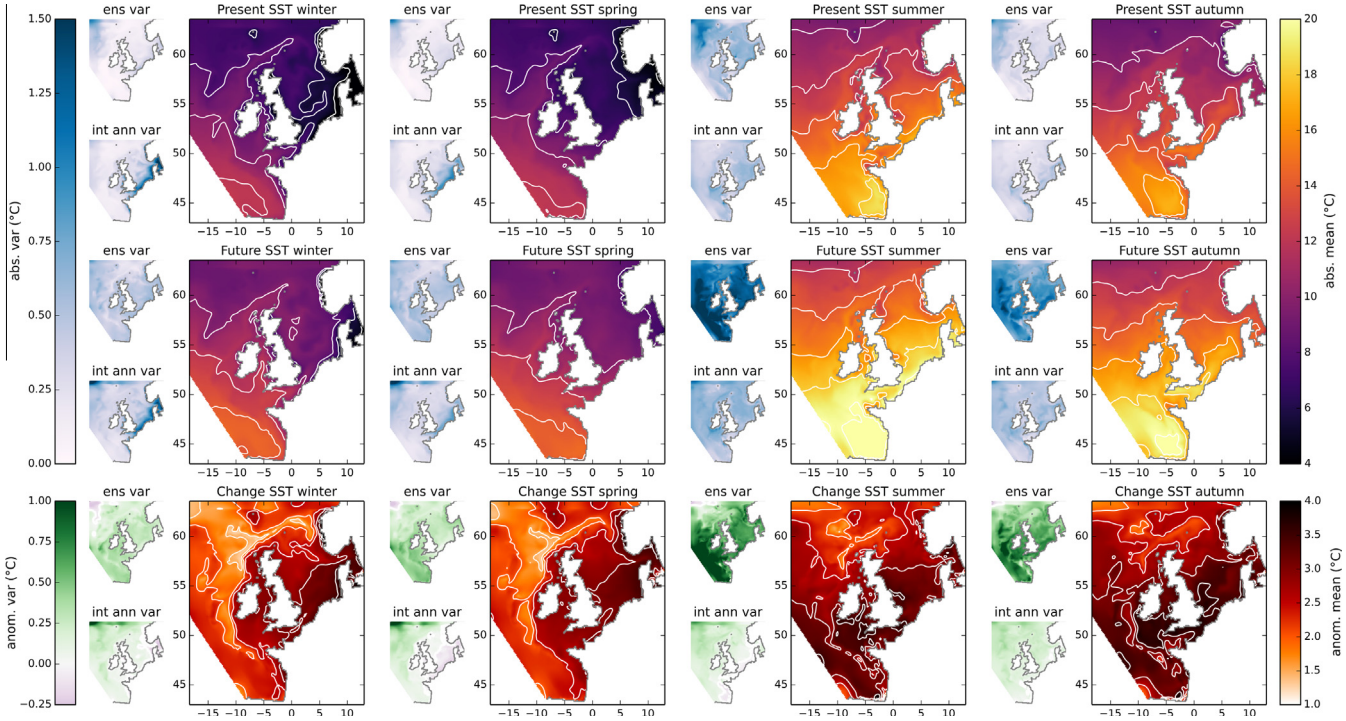

Fig. 4. Projections of SST: The ensemble mean (with 30-year interannual variance σ^2_{int} and ensemble variance σ^2_{ens}) present day (1960–1989; upper row), future (2070–2098, middle row) and difference (bottom row) are plotted for each season (winter: December-February; spring: March–May; summer: June–August; autumn: September–November). Each main plot, representing the ensemble mean, is accompanied (to the left) by the two components of ensemble variance: the interannual variance, σ^2_{int} (labelled int ann var, small lower panel) which is the mean of the interannual variance of each ensemble member; and the ensemble variance, σ^2_{ens}, the variance of the 30-year mean of the 11 ensemble members (labelled ens var, small upper panel). These add linearly to give the total variance associated with the 30-year period across the ensemble, while the square-root of σ^2_{ens}, gives the ensemble standard deviation (not shown).

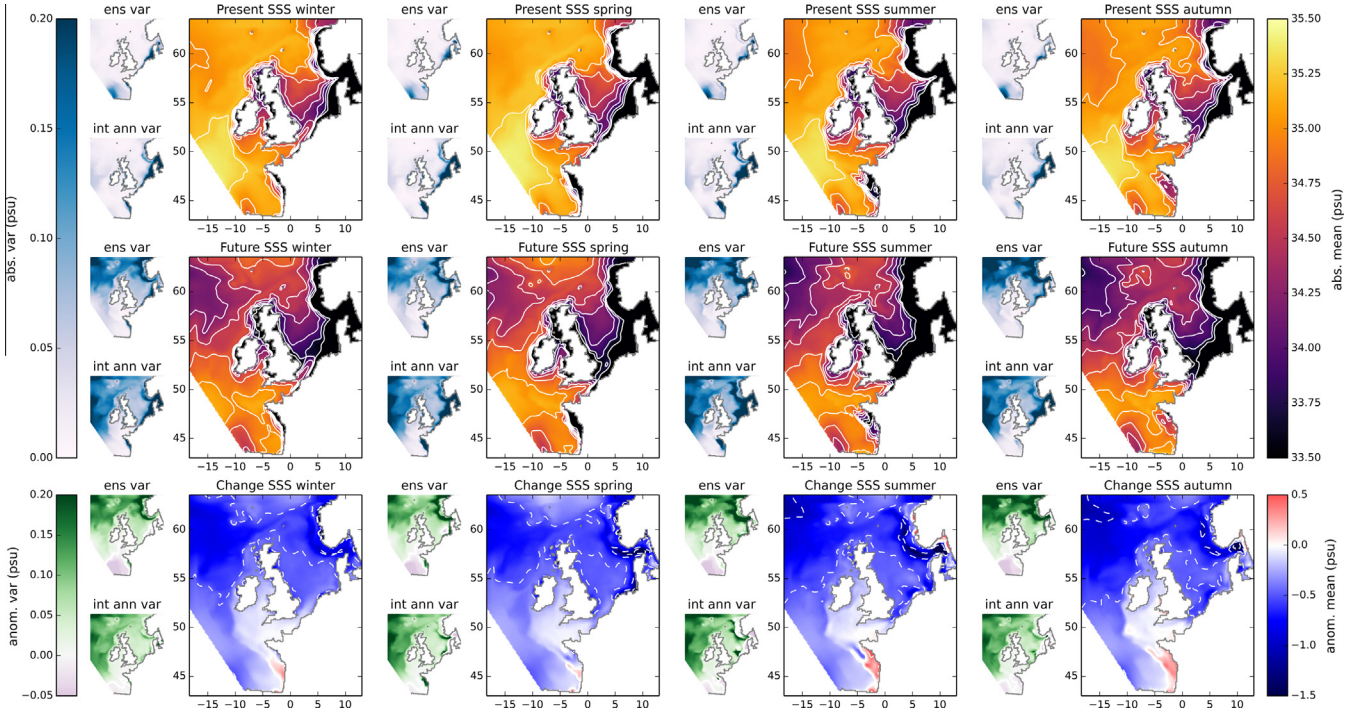

Fig. 5. Projections of SSS, see Fig. 4 for details.

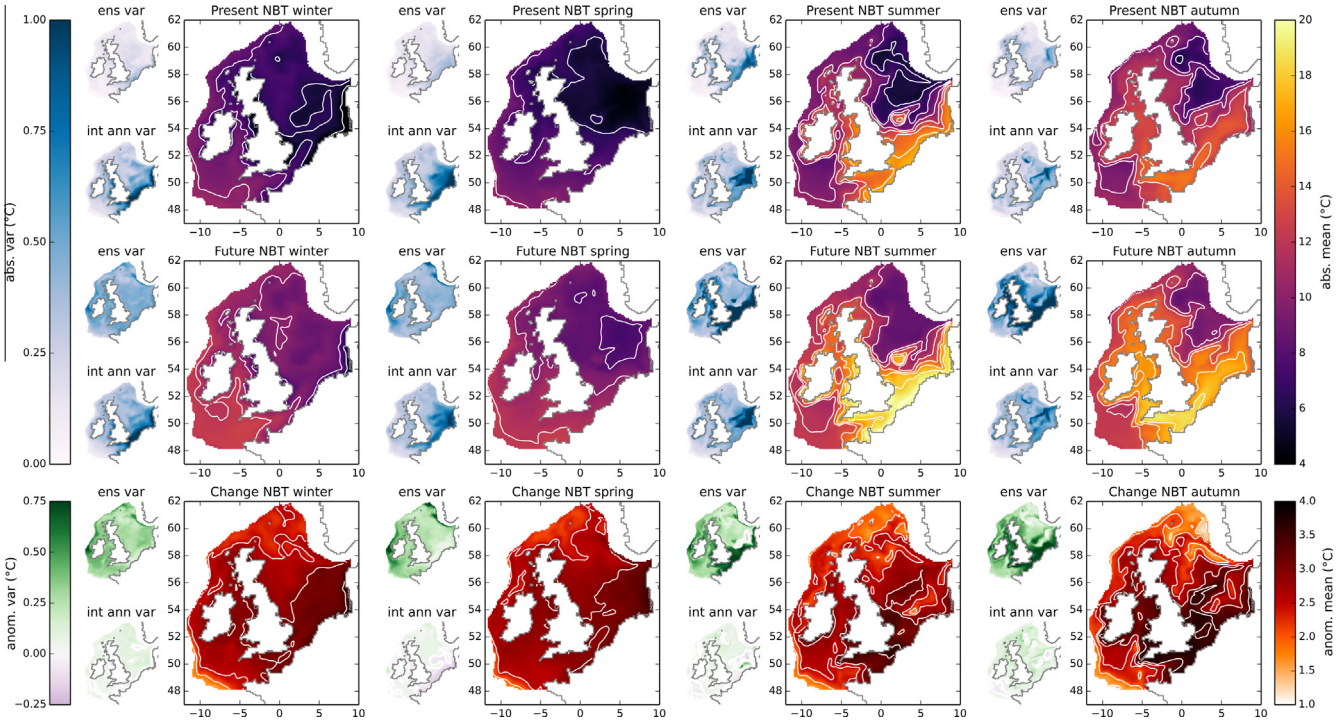

Fig. 6. Projections of NBT, see Fig. 4 for details.

(±2σ = 0.08 psu)). Present day SSS ensemble and interannual variances are fairly low across the shelf (Fig. 5 and, for the Shetland Shelf, Fig. 2), with the exception of the southern North Sea (Fig. 2), German Bight and the Skagerrak. The salinity structure at the boundaries changes considerably during the course of the 21st century, with freshening of the upper ~ 150 m, particularly in the northwest corner of the domain (e.g. the upper 150 m of the western boundary, north of 58°N freshens by 0.76 psu for the ensemble mean), and a general increase in salinity between 150 and 1150 m (the ensemble mean typically increase by ~0.2 psu, with the exception of the eastern part of the northern boundary, which shows a small decrease of 0.06 psu).

Within the model domain the shelf salinity diverges across the ensemble in the future period, with the three ensemble members with the highest ECS (ens_08–10) showing much greater freshening than the rest of the ensemble (Fig. 2). This distinction accompanies the notable change in the circulation configuration also evident for these high ECS members and illustrated in Fig. 3. Despite this apparent bifurcation, however, the ensemble salinity changes are not inconsistent with a normal distribution (according to the Sharpiro-Wilks test at the 5% level); this may be due to the small sample size. The greater freshening for the ens_08-10 members is more pronounced in the outer shelf regions and for these regions it appears to originate in the ocean boundary conditions to the NW of the domain. In the eastern North Sea and the NT, the ensemble variance is related to the change in circulation pattern for the high ECS ensemble members: here some ensemble members tend to receive water from the relatively saline North Atlantic while others receive relatively fresh water from the Baltic (due to the differences in the 'mean present-day' and 'future high-ECS' circulation patterns in Fig. 3). Interannual salinity variability in the NW boundary forcings increases in conjunction with the mean freshening for ens_08-10. These variations are apparently also advected onto the shelf. On the shelf there are therefore widespread increases in both ensemble and interannual variance which are particularly apparent in the northwest of the domain and also in the eastern North Sea and NT. In certain coastal regions, the riverine forcings are also a considerable source of interannual and ensemble variance (such as on the Armorican Shelf).

3.4. Water column stratification and the mixed layer depth

During the winter, the entire shelf (apart from around Norway and the Kattegat) is fully mixed. This changes little over the projection period, and over the ensemble. However, the summer stratification (in terms of PEA; Fig. 7) increases by 20–40% over the projected period for most of the shelf (excluding the region in the vicinity of the NT and the Dooley current). Off the shelf the PEA also significantly increases. In most regions on the shelf, the thermal PEA component, PEAT, dominates the present day seasonal stratification and increases in the projections. The NT behaves differently, however, and has year round salinity stratification, which is greater than the seasonal summer thermal stratification (for example, the maximum present day seasonal NT PEAT (63.91 J/m^3), which occurs in summer is less that the weakest NT PEAS (86.37 J/m^3 in winter); the increase in stratification here is also dominated by PEAS (e.g. the annual mean NT PEAT increases by 0.29 J/m^3 while PEAS increase by 76.16 J/m^3). Off the shelf almost all the increase in PEA is due to salinity (likely due to the strengthening of the HadCM3 halocline).

Most of the shelf has a summer Mixed Layer Depth (MLD) of <20 m (e.g. 15.06 m ensemble mean in northern North Sea with, 2σ = 1.41 m). Most of the shelf regions show very little change in the ensemble mean MLD over the projection period (the summer MLD of most shelf regions shoals by <1 m between the present day and the future period). There is little ensemble spread in the MLD on the shelf (present-day summer shelf-mean MLD 2σ = 0.5 m), and this is similar to the projected change (summer ensemble and shelf mean MLD change is 0.86 m.

4. Discussion

4.1. Significance of the projected changes

In order to assess the significance of the projected changes, we have assessed the results against the high- (inter-annual) and low-frequency variability in the simulations. We have taken the regional mean time-series for the present day (1960–1989) and future period (2069–2098) for each variable, region and ensemble member, and tested whether the difference between them is significant with a *t*-test at the 5% level. From this we can give spatial maps showing which proportion of the ensemble has a significant change (Fig. 8). We find that the projected SST and NBT changes are significant for the entire ensemble, across the domain, given the inter-annual variability, as is the SSS for the northern part of the domain. For the Irish Sea and English Channel, the change is significant for 90% of the ensemble, and 81% for the southern North Sea, Celtic Sea and North Atlantic (South) regions. Only 54% of the ensemble have significant changes in SSS on the Armorican shelf. The NBS has a similar pattern and values to SSS. The PEA changes are significant given the inter-annual variability for most of the ensemble and for most regions, with the exception of the southern North Sea, which is well mixed throughout the year. The projected

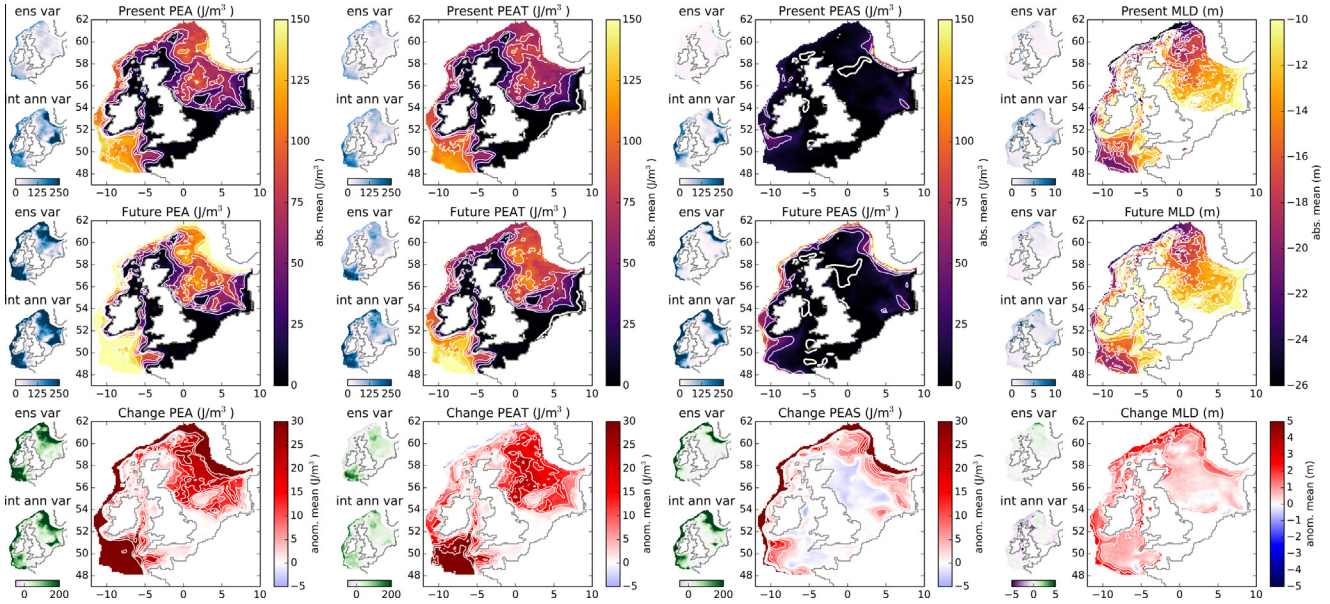

Fig. 7. Summer Projections of PEA, PEAT and PEAS and MLD, see Fig. 4 for details.

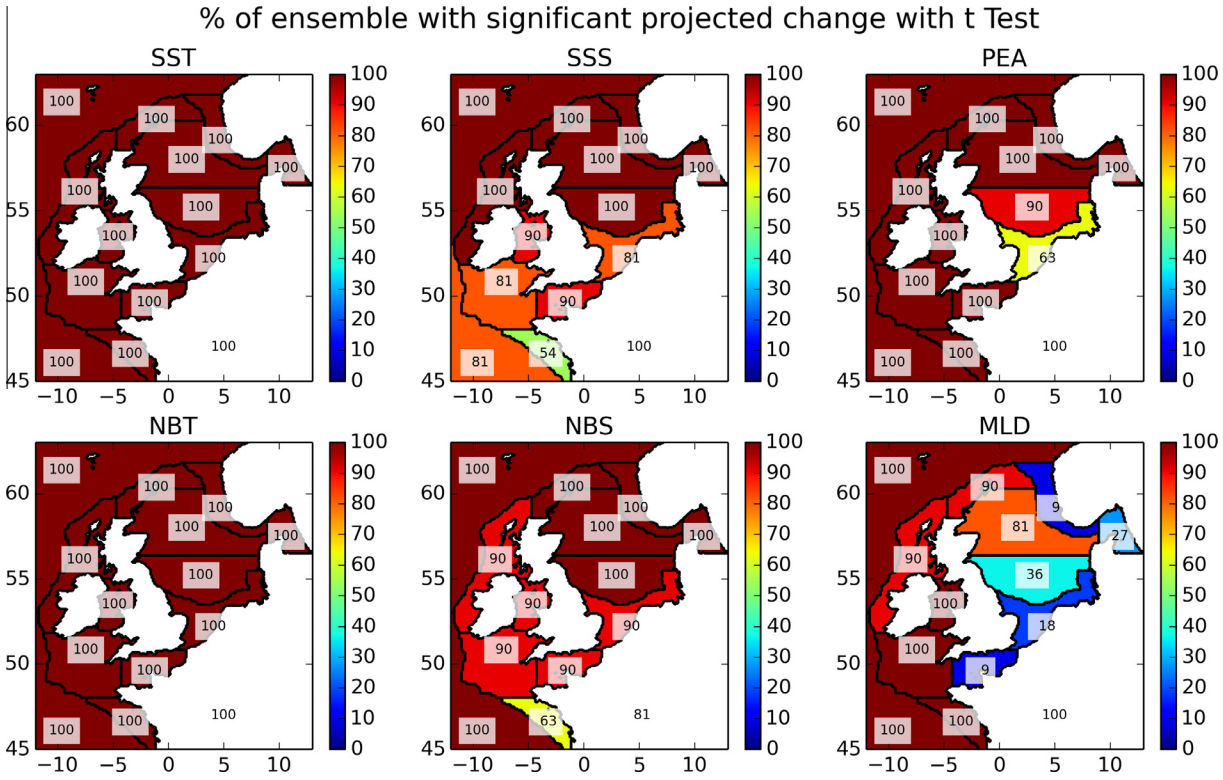

Fig. 8. Significance of projected changes given the high-frequency interannual variability: the percentage of the ensemble where the projected changes are significant with a *t*-test.

changes in MLD are insignificant for most of the ensemble for the English Channel, southern and central North Sea, Skagerrak and Kattegat, and Norwegian Trench, and this reflects the magnitude of the inter-annual variability given the small projected changes. Note that most of the southern North Sea and English Channel are well mixed throughout the year.

However, low-frequency variability may increase or decrease the 30-year mean for the present day or future period, which may increase or decrease the projected change using the time-slice approach. We now assess whether differences we have found to be significant given the high-frequency variability with the *t*-test are robust in the presence of low-frequency variability, by comparing this signal to the noise of the low frequency variability. It is not entirely clear how to divide time-varying changes over the century between climate change and low frequency variability. Here we fit the annual- and regional-mean 147-year transient time-series with a second-order polynomial (ignoring the 1952–1960 spin-up period) to represent the climate change signal, with the low frequency variability represented by 5 non-overlapping 28-year means (discarding the first 7 years as spin-up) for each of the 11 ensemble members, giving 55 samples across the ensemble. We then calculate the standard deviation of these samples, as a measure of the low frequency variability that is representative of the ensemble as a whole. We note that possible auto-correlation of the times-series may restrict the variance, and so calculate the Variance Inflation Factor (VIF):

$$\mathrm{VIF} = \frac{1}{(1-\rho^2)}$$

where ρ is the lag-1 autocorrelation. For this we have concatenated the first 4 28-year means from each ensemble member into one dataset and the last 4 28-year means into another dataset and calculated the Pearson's correlation coefficient between them (ρ). The standard deviation from the 55 28-year means, is then multiplied by VIF to give the estimate of the low-frequency variability. However, due to the low number of samples, potential differences in low-frequency variability between ensemble members, the method used to remove the trend, and possible changes in low-frequency variability over time, we may have under- or over-estimated this variance.

The climate change signal is taken as the difference between the 1960–1989 and 2069–2098 means from the polynomial fit. Where this difference is greater than 1.96 times the inflated standard deviation of the low-frequency variability, we consider the projected change to be robust. This is repeated for all variables, regions and ensemble members. The number of ensemble members with a robust change for each region is presented in Fig. 9 as a percentage (for SST, NBT, SSS, NBS, PEA and MLD).

The changes in SST and NBT are significant given the low-frequency variability, as also found for the high frequency variability. The projected SSS changes over most of the northern part of the shelf are still significant for most if not all the ensemble. A few more ensemble members in the western portion of the shelf (Irish Sea and shelf, Celtic Sea and English Channel) have low signal-to-noise ratios, and so the significance of the change found with the *t*-test could have come from the considerable low-frequency variability. However, over most of the shelf seas in excess of 70% of the ensemble still exhibits changes that we consider significant, given the low- and high- frequency variability; areas where this does not apply are in the English Channel (63%) and the Armorican Shelf (54%). Interestingly one ensemble member that exhibited an insignificant change with the *t*-test was found to have a high signal-to-noise ratio, reflecting considerable inter-annual variability, but little low-frequency variability. Most of the projected changes in PEA are significant across the ensemble, and again little low-frequency variability in the southern North Sea results in an increase to 90% of the ensemble having a significant signal-to-noise ratio. There is very little low-frequency variability of the

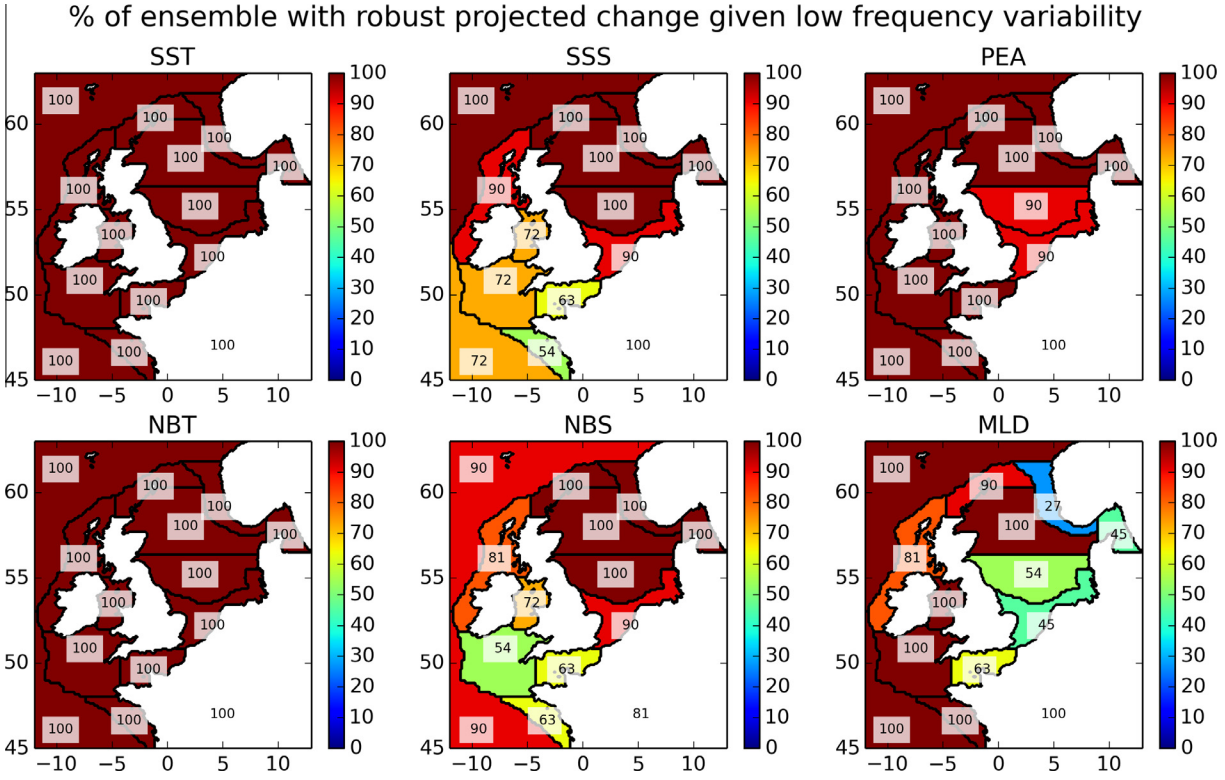

Fig. 9. Robustness of projected changes given the low-frequency variability: the percentage of the ensemble that have projected changes that are greater than the low-frequency variability (1.96 times the standard deviation).

MLD in the North Sea, English Channel, Skagerrak/Kattegat and Norwegian Trench despite the considerable high-frequency variability, and so more of the ensemble appears to have a significant signal-to-noise ratio than has a significant change given the *t*-test.

4.2. Comparison with projections of Holt et al. (2010)

The projections presented in this study are closely related to the single projection of Holt et al. (2010), but we have made significant methodological improvements. The time-slice approach of Holt et al. (2010) and the limitation of a single projection, which used forcing from unperturbed parameter member of our forcing ensemble, ens_00, makes their results more susceptible to bias due to interannual/decadal variability. The ens_00 projection includes a particularly cold decade: the North Sea annual mean SST is ~ 1 °C cooler in our ens_00 projection than in our ensemble mean for the 2080s, and the Holt et al. (2010) 2080–2090 mean is below our ensemble-mean minus 2σ (not shown). When comparing the normalised position of the Holt et al. (2010) projected change in SST (and NBT) (2070–2098 relative to 1961–1990) within our ensemble (Holt et al. (2010) value minus ensemble mean, divided by the ensemble standard deviation), we find that the Holt et al. (2010) SST projection is in the lower half of the ensemble, typically between 0.5 and 1.0 ensemble standard deviations below the ensemble mean across the shelf (Fig. 10). Looking at our full transient projection for ens_00 (not shown) indicates that this is due to low frequency variability about the long term trend. Our ensemble approach allows the uncorrelated phases of such long-period variability to be at least partially averaged out across the ensemble, reducing the likelihood of such a bias. Furthermore we have shown where such low frequency variability affects the projections.

The differences between our projected SSS change and that of Holt et al. (2010) are more striking than for SST. Holt et al. (2010) projected a freshening change in shelf SSS of −0.19 psu, whereas our ensemble mean projects a much larger freshening, of −0.41 psu ($\pm 2\sigma$ = 0.47 psu). The Holt et al. (2010) value is about 1 standard deviation more saline than the ensemble mean projected SSS change (Fig. 10). As we have noted previously, the future oceanic forcings used by Holt et al. (2010) consisted of the addition of a single edge-of-shelf-break-averaged salinity change profile to the present day boundary conditions. These values were then applied further offshore. The freshening in the vicinity of Greenland was therefore not applied and other spatial variations were neglected (e.g. our ensemble-mean SSS freshening in the boundary of the northwest corner is ~0.5 psu whereas in the south it is ~0.2 psu, with much greater change in the more extreme members). Much of the shelf freshening in our ensemble is linked to freshening of the northern ocean boundary conditions. Furthermore our ensemble approach has suggested considerable uncertainty in the salinity changes with an apparent bifurcation of our ensemble freshening, with a group of three ensemble members undergoing notably more freshening than the other members, driven by a corresponding greater freshening in their boundary forcings. The Celtic/Irish Sea water behaves differently in terms of salinity change, as their water tends to originate from further south, with a much slower exchange rate with the open ocean (Holt et al., 2012), and so is less influenced by the fresh northern oceanic boundary water.

4.3. Relationship of projected shelf changes to the large-scale forcings

The underlying QUMP PPE was designed to span uncertainty in large-scale climate change, as represented by ECS, and with the ensemble generated by varying uncertain parameters within the HadCM3 atmosphere model parameterisation schemes. As we have noted, ECS is a representation of global climate change and may not be the most relevant index for spanning uncertainty in the

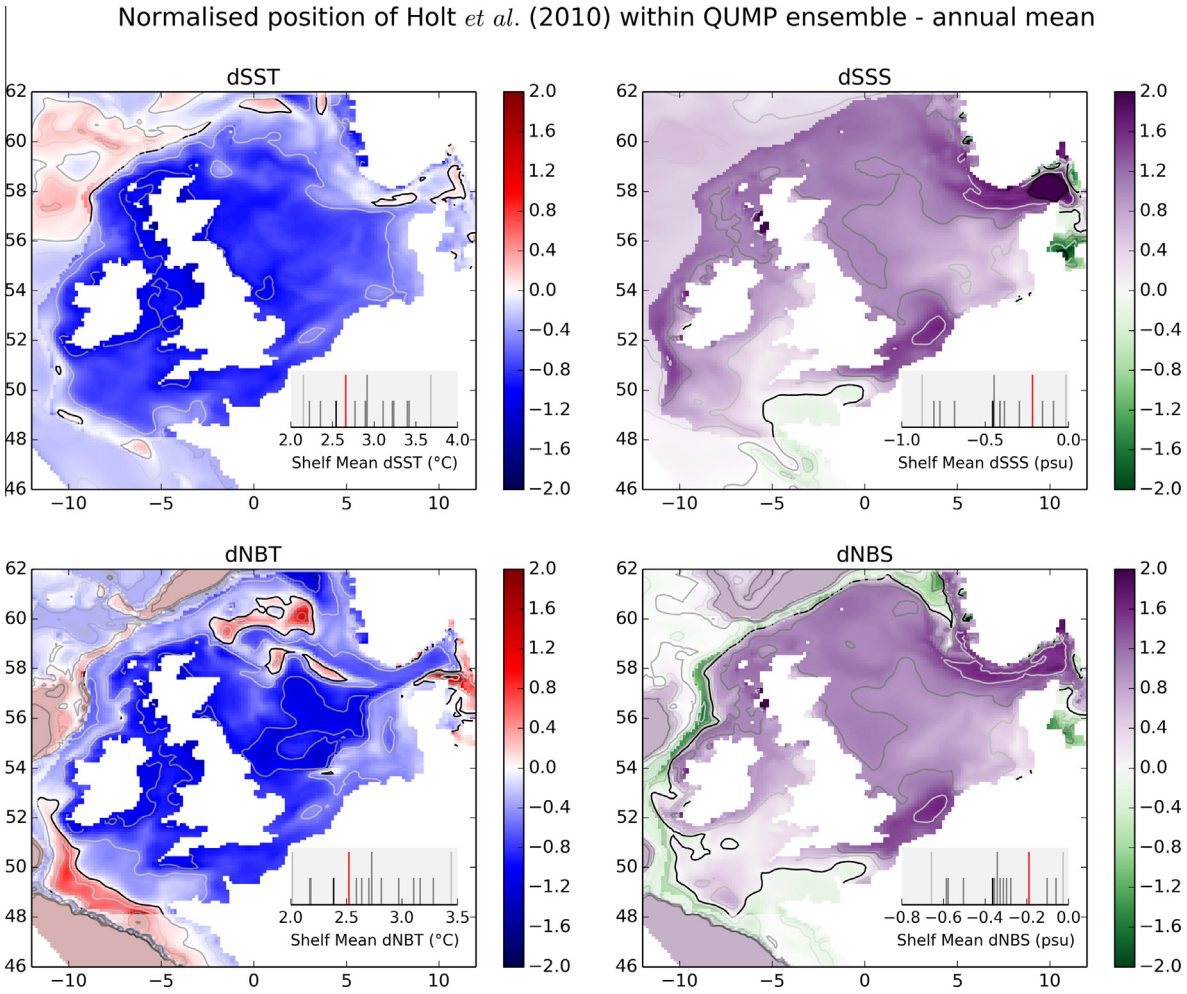

Fig. 10. Normalised position of the Holt et al. (2010) shelf temperature (SST and NBT) and salinity (SSS and NBS) projections (2070–2098 relative to 1961–1990) within out ensemble of projections (2069–2098 relative to 1960–1989). The maps show the Holt et al. (2010) projections minus our ensemble mean divided by the ensemble standard deviation, and so a value of zero suggests that the Holt et al. (2010) and our ensemble mean are the same, while a value of 1 suggest that the Holt et al. (2010) is one ensemble standard deviation above our ensemble mean projection. The black contours denote values of 0 and ±1.96, while the grey contours dente ±0.5, ±1.0 and ±1.5. Values off the shelf are greyed out. The temperature projections are generally negative, suggesting UKCP09 projects less warming the ensemble mean (shown as blue), while the Holt et al. (2010) salinity projections are generally positive, suggesting that the Holt et al. (2010) projections have greater values of dSSS than the ensemble mean, however, as the ensemble mean shows a freshening (negative values of dSSS), Holt et al. (2010) having a greater dSSS than the ensemble mean suggests it has less freshening (and so projects a more saline future, shown as purple). This is clarified in the subplots associated with each panel. These show the absolute shelf mean change in SSS (or SST, NBT, NBS) for the 11 ensemble member (grey short lines, with ens_00 in black) with the ensemble mean and ±1.96 ensemble standard deviations in the grey tall lines. The UKCP09 value is shown in red).

NWE shelf seas regional climate. However, we have already noted that the high ECS ensemble members show the greatest NWE shelf sea freshening, and also greatest change in the circulation configuration. Further analysis shows that high ECS projections also tend to show the greatest shelf warming (Table 1).

To investigate the association between shelf sea changes and large-scale climate change further, we have summarised the projected shelf seas changes for each ensemble member into annual-and-shelf-mean changes in SST and SSS, together with a measure of how the shelf circulation changes into the future period. Large-scale climate change is characterised for each ensemble member using a number of measures, including measures of atmospheric and surface oceanic change and change in relevant climate indices. The climate indices considered include changes in the winter North Atlantic Oscillation (NAO), the Atlantic Multidecadal Oscillation (AMO), the Atlantic Meridional Overturning Circulation (AMOC) and the strength and location of the European storm track. NAO, AMO and AMOC are all calculated from the global fields for each ensemble member of the QUMP PPE. The NAO index is calculated as the surface pressure difference between the Azores (Ponta Delgada) and Iceland (Stykkishólmur) averaged from December to February. AMO is the low-pass filtered (with a Chebyshev recursive filter) difference between the global and North Atlantic mean (0–60°N, 0–80°W) SST anomaly (relative to 1952–2000 mean) (adapted from Sutton and Dong, 2012). AMOC is the strength of the maximum North Atlantic overturning stream function calculated between 35°N and 65°N. The European storm-track location and strength is identified from the band-pass filtered mean sea-level pressure along the 4°W meridian (Lowe et al., 2009).

The correlations between ECS and the projected shelf changes across the ensemble are significant for SST (0.93), SSS (−0.70) and for the change in future circulation (0.90), supporting the choice of ECS to underpin the global QUMP PPE even for this smaller scale aspect of climate change (Table 6). When looking at the spread of projected changes in SST on the shelf, we find very strong correlations with change in SAT at all the spatial scales considered. There is no significant correlation with any other driving climate index, apart from the change in AMO. The correlations with the change in salinity are more subtle. Potentially, a correlation might be expected between shelf SSS and the precipitation minus

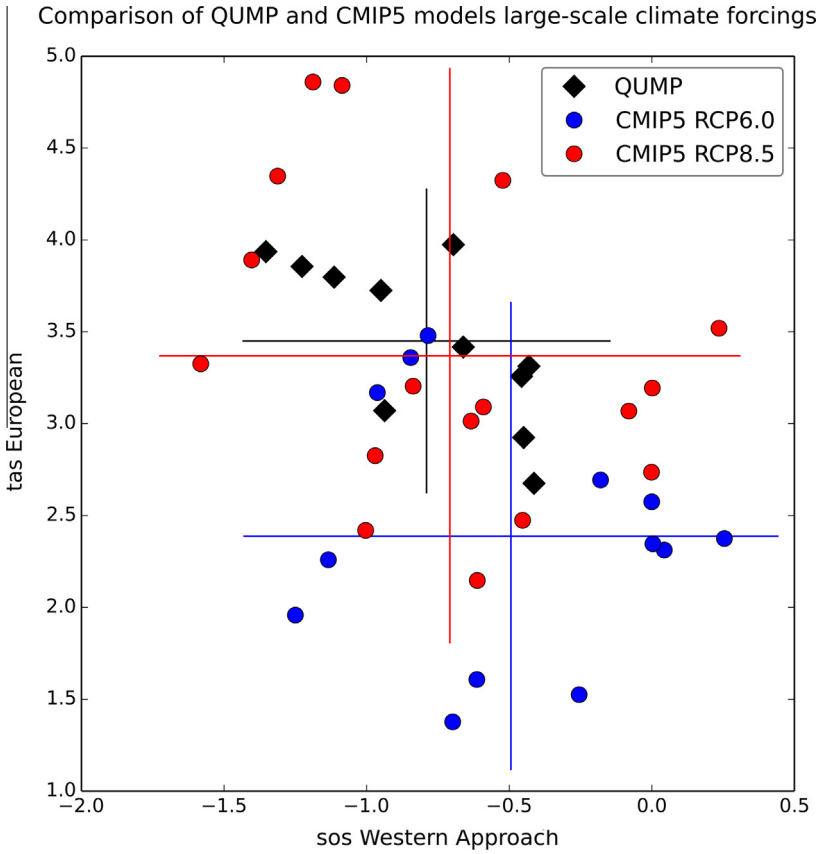

Fig. 11. Comparison of QUMP ensemble (black diamonds) to CMIP5 models (RCP6.0: blue circles; RCP8.5: red circles) in terms of change in European model domain near surface air temperature (tas), and change in oceanic surface salinity (sos) in the western approach to Europe (50–60°N, 40–10°W). The change is between the present day (1960–1989) and the future period (2069–2098). The CMIP5 models for both emission scenarios are: CESM1-CAM5, CSIRO-Mk3-6-0, GFDL-ESM2G, GISS-E2-H, GISS-E2-R, HadGEM2-AO, HadGEM2-ES, IPSL-CM5A-LR, MIROC-ESM, MIROC-ESM-CHEM, MIROC5, NorESM1-M, NorESM1-ME. RCP8.5 additionally includes: CNRM-CM5, EC-EARTH, IPSL-CM5A-MR, MPI-ESM-LR.

evaporation when averaged over the Atlantic, if this latter field substantially controls the changes in Atlantic salinity entering the shelf sea domain, however this correlation was not found to be significant (0.34 – not shown in Table 6). The surface salinity in the western approach to the European domain (40–10°W, 50–60°N), however, is very significantly correlated to dSSS ($r = 0.92$), possibly indicating a role for the larger scale ocean circulation in controlling salinity changes in the shelf seas. The changes in the future shelf sea circulation pattern that we showed earlier (Fig. 3) are quantified, by correlating each of the 11 ensemble member future circulation patterns with both the 'future high-ECS' mean pattern (we term this set of 11 correlations as dCircF), and the "Mean Present-Day" mean pattern (dCircP), using a spatial vector correlation coefficient (Crosby et al., 1993). We find significant positive (negative) correlations between dCircF (dCircP) with ECS, with Global and European Surface Air Temperature.

We can use these relationships to speculate how well these projections capture the spread in change of shelf SST and SSS compared to a hypothetical set of projections that could have been run forced by the more recent CMIP5 models (run under different emission scenarios). Such relationships may also help identify a sub-set of models within the current CMIP5 ensemble to downscale, that may produce the greatest range of changes on the shelf, albeit with the caveat that the relationships were identified from a single model forcing ensemble. We use change in European surface air temperature (as a proxy for change in SST and circulation) and change in salinity in the western approach (40–10°W, 50–60°N) as a proxy for change in shelf salinity. These two proxies are used as a pair of indices to aid our understanding of potential uncertainty in shelf sea projected changes given by downscaling the QUMP ensemble compared to that which might be given by downscaling CMIP5 models (Fig. 11).

The change in European surface air temperature across the QUMP ensemble falls within the range of the CMIP5 RCP8.5 MME, with QUMP having a similar mean, but less spread; this field generally warms more in QUMP than in the RCP6.0 ensemble. The Western Approach salinity also agrees fairly well with both CMIP5 ensembles, with similar freshening to RCP8.5 (RCP6.0 exhibits slightly less freshening), although both CMIP5 ensemble show greater spread than QUMP. We conclude that the QUMP PPE falls within the range of the CMIP5 RCP8.5 MME, in terms of mean change, although the greater spread of these CMIP5 ensembles means that some MME member exhibit greater or lesser change than that of the QUMP ensemble. The differences in spread between the QUMP PPE and the CMIP5 MME, and the differences between the emission scenarios, suggest that model structural uncertainty and emission scenario uncertainty are likely to be important components of uncertainty in climate projections of the NWE shelf seas. Future studies of uncertainty in shelf seas projections should assess how this structural uncertainty of the CMIP5 MME, and the emission scenario uncertainty, propagates into the shelf seas, and how it compares to the model parameter uncertainty quantified here.

5. Summary and conclusions

This study provides a set of projections of how the hydrodynamic conditions on the NW European Shelf might respond to

climate change. It responds to a substantial increase in the demand for evidence-based policy advice for marine climate change. From a UK perspective the Climate Change Act (2008), and the ensuing 5-yearly Climate Change Risk Assessments (CCRA) provide a statutory obligation to assess the impact of climate change on the UK. In this section we consider our projections and their spread and compare to the other shelf seas climate projections, including those of Holt et al. (2010), on which they were based. We consider whether the projected changes are significant given high frequency (interannual) and low frequency variability in the various quantities. We also consider the relationship between the projected spread in shelf sea quantities and measures of large scale changes in the forcing, including ECS and other drivers.

The climate projections we have produced for the NWE shelf seas are based on an ensemble of transient simulations. This approach allows a more robust central estimate of climate change than is possible from either a deterministic or time-slice methodology, which are more susceptible to bias from natural variability. Furthermore, the ensemble approach allows a quantification of aspects of uncertainty, in our case relating to uncertainty arising from the large-scale climate. The projections in this study build on the methodology of Holt et al. (2010) who gave a single shelf seas projection driven by one of our global projection ensemble members. The uncertainty range provided by our ensemble approach, together with the more self-consistent atmosphere and ocean forcings used, and the full-transient-simulation rather than time-slice approach, considerably advance these projections. Our shelf sea ensemble is forced by an 11-member global projection PPE under the SRES A1B scenario, downscaled by a regional model for the atmospheric forcing. The global PPE was designed to span the range of ECS associated with uncertainty in atmospheric parameters within the driving GCM (representing uncertainty in global climate). While a wide range of ECS is appropriate for uncertainty in global climate projections, it is not so immediately apparent that it is also a useful measure of uncertainty for the regional NWE shelf sea projections. However, this study has found that many aspects of the shelf sea projections, notably some changes in temperature, circulation and salinity, do appear to be strongly related to ECS, implying that this is a useful selection index for the global driving projections. This study provides an improved estimate of uncertainty for NWE shelf sea projections. Other sources of uncertainty which we have discussed, but which are outside the scope of this study, include model structural uncertainty (both of the forcing model and of the shelf seas model), emission scenario uncertainty, and that of choice of the forcing methodology.

In the projections presented in this study we have found a spatially and temporally varying warming of the NWE shelf seas, with an ensemble and shelf mean SST warming of 2.90 °C (for 2069–2098 relative to the 1960–1989 baseline) and an ensemble spread of $2\sigma = 0.82$ °C, this is slightly warmer than that of Holt et al. (2010) (2.62 °C for the same region). We find an ensemble, annual and shelf mean change in SSS of −0.41 psu (freshening) over the same period with an ensemble spread of $2\sigma = 0.47$ psu. In the future there is a divergence in the ensemble in terms of the salinity change, with high ECS ensemble members exhibiting a much greater freshening than members with a lower ECS. The ensemble mean freshening projected here is greater than that of Holt et al. (2010) due to an improved treatment of the oceanic boundary conditions. We have projected little change in the spatial extent of stratification but an increase in its strength (as measure by PEA). There was little change in the mixed layer depth.

There is considerable spatial heterogeneity to these changes. We find that there is a change in the circulation configuration in the high ECS ensemble members, particularly within the North Sea, and NT. The greatest winter/spring warming is in the southwest North Sea, and summer/autumn warming in the Celtic Sea and North Sea. The area of the shelf current extension (57°N, 10°W to 62°N, 5°E) typically shows less warming (1–2 °C), associated with a weakening shelf break extension current (which reduces from 2.30 Sv ($\pm 2\sigma = 0.37$ Sv) to 1.05 Sv ($\pm 2\sigma = 1.73$ Sv) at 56°N). Due to the shelf being fully mixed in the winter (with the exception of the NT and Skagerrak/Kattegat which are salinity stratified), there is no particular difference in surface warming in stratified and mixed regions on the annual timescale, although there tends to be a greater NBT warming in permanently mixed regions. The pattern of salinity change is much more complex, due to its greater reliance on advective processes. Typically the German Bight and NT show the greatest surface freshening, and the Celtic Sea shows little change in salinity relative to the present day.

Our ensemble projections incorporate spread in an annual mean projection arising from both ensemble variance and interannual variance. These two terms are often driven by different processes, for example, changes in the ensemble spread could be due to different ECS values across the different ensemble members, while interannual variability may change with global warming due to changes in climate processes and feedbacks (Boer, 2009). Due to the use of flux adjustments within the underlying PPE, the present day ensemble spread may be reduced, and these variance terms are not compared in the present day. For SST, the interannual variance undergoes little change into the future, while for some regions the SSS interannual variance increase is substantial. The ensemble variance tends to be relatively small for the present day time periods of the simulations (likely constrained by the flux adjustment of the forcing simulations) and increases into the future as the ensemble members diverge. The relative magnitudes of the ensemble variance and the interannual variance differ for temperature and salinity. In the future projections, the interannual variance is generally greater than the ensemble variance, but this is not always the case (with future summer SST being an example).

There is an apparent divergence in the behaviour of the ensemble, particularly in terms of salinity and the circulation configuration. The ensemble members with the highest climate sensitivity (ens_08-10) tend to show much greater changes (relative to present day) compared to the lower climate sensitivity members. This is consistent with the difference in freshening of the salinity in the ocean boundary forcings (to the NW of the domain) across the ensemble. The change in circulation and salinity are closely related, and are likely to be self-reinforcing. Despite the divergence in salinity, the ensemble is still statistically normal, however this should be considered when using the salinity ensemble mean.

Our projections tend to give a greater warming than other studies within the literature. Ådlandsvik (2008) projected a mean SST warming of 1.7 °C between 1972–1997 and 2072–2097 for the North Sea, under the SRES A1B scenario. Their projected SST change varied spatially, ranging from 1 to 2.5 °C, with the greatest warming occurring in the summer southwest North Sea, and southeast North Sea in the autumn. There was much weaker warming in the northwest of the North Sea, and in the open ocean. During the same period we project an annual mean North Sea average (using a similar North Sea mask) SST warming of 2.94 °C ($\pm 2\sigma = 0.7$ °C). Thus, the ensemble-mean warming is greater in our projections than in Ådlandsvik (2008) and the uncertainty given by our ensemble spread does not encompasses their projection. The Irish Sea transient projections (under SRES A1B) of Olbert et al. (2012) also show weaker warming than in our projection. By fitting a linear trend to the SST from their 120 year transient experiments, they project a 1.89 °C rise in temperature between 1980s and 2090s. By comparison, when we fit a linear trend to a similar regional mean (51.0–56.0°N, 7.0–2.5°W) we find a 110 yr warming (from 1985 to 2095) of 2.94 °C ($\pm 2\sigma = 0.88$ °C). A recent study by

Mathis and Pohlmann (2014) used median regression analysis on their transient experiments (1951–2099) to calculate the trends in temperature and salinity, and to assess their significance given the low frequency variability captured within their simulations. Their study (run under the SRES A1B emissions scenario) suggests that annual mean SST will increase with a trend of 1.8 °C/100 yr. With a similar domain and approach, we project a warming 2.57 °C ($\pm 2\sigma = 0.68$ °C). They also project a SSS trend of −0.6 psu/100 yr which is in agreement with our projections (−0.49 psu/100 yr, $\pm 2\sigma = 0.47$ psu). The greater projected surface warming from these studies could have a number of reasons: different heat fluxes into the shelf seas (surface and lateral), different responses to these heat fluxes, or even different vertical distribution of heat within the shelf seas. Both Olbert et al. (2012) and Mathis and Pohlmann (2014) were driven by ECHAM5 and MPI/OM under the SRES A1B scenario (with different shelf seas models) which may explain why both have a weaker warming than in our study.

Impacts studies that wish to understand how the marine ecosystem may change into the future rely on the underlying projections of the physical environment. At present, the available information on the likely changes is limited (MCCIP, 2012; Pinnegar et al., 2012). The ensemble presented in this study can inform impact studies, with an uncertainty estimate for the projected changes, even if this is used in a simple way, for example with exemplar ensemble members that give the greatest and weakest changes, or with the ensemble mean and spread. We have not weighted any of the ensemble members in terms of their being more or less likely outcomes, and we do not consider the ensemble mean to be the most likely future (we consider each ensemble member to be equally likely). However the ensemble mean together with the ensemble spread is a convenient summary statistic to describe the distribution of the ensemble.

In conclusion, we have developed an ensemble modelling system and have started to investigate the uncertainty in the simulated changes in the NWE shelf seas at spatial scales relevant to impacts around the UK. We have assessed the significance of the projected changes, given low- and high-frequency variability. We have also considered how the response of the shelf relates to the driving GCM forcings, and compared how key GCM parameters from our ensemble compare to the CMIP5 RCP6.0 and RCP8.5 MME. This study is an important first step towards quantifying uncertainty in shelf seas climate projections, but future studies are required to investigate other sources of uncertainty.

6. Data Release

A subset of the data used in this paper (including the data used to produce figures 4–7) are available to download from the Centre for Environmental Data Analysis: http://catalogue.ceda.ac.uk/uuid/9eba512621144dbaacda1ddb470f885b.

These data include spatial maps of surface and bed, temperature and salinity, and the potential energy anomaly and the mixed layer depth. The data are for 30-year periods of the present day (1960–1989), future period (2069–2098) and the difference between these two periods. We have provided the ensemble mean, ensemble variance, ensemble standard deviation, interannual variance (DOI: 10.5285/76defc55-c384-4fbd-863a-84ccf60c1375), and three exemplar ensemble members (DOI: 10.5285/b85e9319-1531-4c93-875b-e6bbc8b7d9ac).

Acknowledgements

The authors thank Sarah Wakelin (NOC) and Pat Hyder (MO) for their support and work in the early part of this study, David Sexton (MO) and Glen Harris (MO) for advice and support with the QUMP PPE, James Hocking (MO) for checking the variance decomposition, Charlotte Pascoe (CEDA) and Ag Stephens (CEDA) for the data release. This work was supported by the Joint DECC/Defra Met Office Hadley Centre Climate Programme (GA01101) and the Minerva Project (ME5213). Holt is supported by the NOC National Capability modelling programme.

Appendix A. Supplementary material

Supplementary data associated with this article can be found, in the online version, at http://dx.doi.org/10.1016/j.pocean.2016.09.003.

References

Ådlandsvik, B., 2008. Marine downscaling of a future climate scenario for the North Sea. Tellus A 60, 451–458.

Andrews, T., Gregory, J.M., Webb, M.J., Taylor, K.E., 2012. Forcing, feedbacks and climate sensitivity in CMIP5 coupled atmosphere-ocean climate models. Geophysical Research Letters 39 (9), L09712. http://dx.doi.org/10.1029/2012GL051607.

Beaugrand, G., Reid, P.C., Ibañez, F., Lindley, J.A., Edwards, M., 2002. Reorganization of North Atlantic marine copepod biodiversity and climate. Science 296 (5573), 1692–1694. http://dx.doi.org/10.1126/science.1071329.

Boer, G.J., 2009. Changes in interannual variability and decadal potential predictability under global warming. Journal of Climate 22, 3098–3109. http://dx.doi.org/10.1175/2008JCLI2835.1.

Collins, M., Booth, B.B.B., Bhaskaran, B., Harris, G.R., Murphy, J.M., Sexton, D.M.H., Webb, M.J., 2011a. Climate model errors, feedbacks and forcings: a comparison of perturbed physics and multi-model ensembles. Climate Dynamics 36 (9–10), 1737–1766. http://dx.doi.org/10.1007/s00382-010-0808-0.

Collins, W.J., Bellouin, N., Doutriaux-Boucher, M., Gedney, N., Halloran, P., Hinton, T., Hughes, J., Jones, C., Joshi, M., Liddicoat, S., Martin, G., O'Connor, F., Rae, J., Senior, C.A., Sitch, S., Totterdell, I.J., Wiltshire, A., Woodward, S., 2011b. Development and evaluation of an Earth-system model – HadGEM2. Geoscience Model Development 4, 1051–1075.

Crosby, D.S., Breaker, L.C., Gemmill, W.H., 1993. A proposed definition for vector correlation in geophysics: theory and application. Journal of Atmospheric and Oceanic Technology 10 (3), 355–367.

Dye, S.R., Hughes, S.L., Holliday, N.P., Kennedy, J., Berry, D.I., Kent, E.C., Inall, M., Kennington, K., Smyth, T., Nolan, G., Tinker, J., Andres, O., Beszczynska-Möller, A., 2013. Climate change impacts on the waters around the UK and Ireland: temperature (Air and Sea). MCCIP Science Review 2013. http://dx.doi.org/10.14465/2013.arc01.001-012.

Gordon, C., Cooper, C., Senior, C.A., Banks, H., Gregory, J.M., Johns, T.C., Mitchell, J.F.B., Wood, R.A., 2000. The simulation of SST, sea ice extents and ocean heat transports in a version of the Hadley Centre coupled model without flux adjustments. Climate Dynamics 16 (2–3), 147–168.

Gröger, M., Maier-Reimer, E., Mikolajewicz, U., Moll, A., Sein, D., 2013. NW European shelf under climate warming: implications for open ocean – shelf exchange, primary production, and carbon absorption. Biogeosciences 10, 3767–3792. http://dx.doi.org/10.5194/bg-10-3767-2013.

Harvey, B.J., Shaffrey, L.C., Woolings, T.J., Zappa, G., Hodges, K.I., 2012. How large are projected 21st century storm track changes? Journal of Geophysical Research 39. http://dx.doi.org/10.1029/2012GL052873.

Hewitt, H.T., Copsey, D., Culverwell, I.D., Harris, C.M., Hill, R.S.R., Keen, A.B., McLaren, A.J., Hunke, E.C., 2011. Design and implementation of the infrastructure of HadGEM3: the next-generation Met Office climate modelling system. Geoscience Model Development 4, 223–253. http://dx.doi.org/10.5194/gmd-4-223-2011.

Holt, J., Allen, I., Proctor, R., Gilbert, F.J., 2005. Error quantification of a high-resolution coupled hydrodynamic-ecosystem coastal-ocean model: Part 1. Model overview and assessment of the hydrodynamics. Journal of Marine Systems 57, 167–188.

Holt, J., Butenschön, M., Wakelin, S., Artioli, Y., Allen, I., 2012. Oceanic controls on the primary production of the northwest European continental shelf: model experiments under recent past conditions and a potential future scenario. Biogeosciences 9, 97–117.

Holt, J., Wakelin, S., Lowe, J.A., Tinker, J., 2010. The potential impacts of climate change on the hydrography of the northwest European continental shelf. Progress in Oceanography 86 (3–4), 361–379. http://dx.doi.org/10.1016/j.pocean.2010.05.003.

Holt, J.T., James, I.D., 2001. An s coordinate density evolving model of the northwest European continental shelf – 1, model description and density structure. Journal of Geophysical Research-Oceans 106 (C7), 14015–14034.

Holt, J.T., James, I.D., Jones, J.E., 2001. An s coordinate density evolving model of the northwest European continental shelf 2, seasonal currents and tides. Journal of Geophysical Research-Oceans 106 (C7), 14035–14053.

Ingleby, B., Huddleston, M., 2007. Quality control of ocean temperature and salinity profiles – historical and real-time data. Journal of Marine Systems 65, 158–175. http://dx.doi.org/10.1016/j.jmarsys.2005.11.019.

IPCC, 2013. Climate Change 2013: The Physical Science Basis. Contribution of Working Group I to the Fifth Assessment Report of the Intergovernmental Panel on Climate Change. Cambridge University Press, Cambridge, United Kingdom and New York, NY, USA.

Jones, R.G., Noguer, M., Hassell, D.C., Hudson, D., Wilson, S.S., Jenkins, G.J., Mitchell, J. F.B., 2004. Generating High Resolution Climate Change Scenarios Using PRECIS. Met Office Hadley Centre, Exeter, UK.

Lowe, J.A., Howard, T.P., Pardaens, A., Tinker, J., Holt, J., Wakelin, S., Milne, G., Leake, J., Wolf, J., Horsburgh, K., Reeder, T., Jenkins, G., Ridley, J., Dye, S., Bradley, S., 2009. UK Climate Projections Science Report: Marine and Coastal Projections. Met Office Hadley Centre, Exeter, UK.

Mathis, M., Pohlmann, H., 2014. Projection of physical conditions in the North Sea for the 21st century. Climate Research 61, 1–17. http://dx.doi.org/10.3354/cr01232.

MCCIP, 2012. Marine Climate Change Impacts Knowledge Gaps, Summary Paper. Buckley, P.J., Dye, S.D., Frost, M., Wallace, C.J. (Eds.), Lowestoft: 8.

Megann, A., Storkey, D., Aksenov, Y., Alderson, S., Calvert, D., Graham, T., Hyder, P., Siddorn, J., Sinha, B., 2014. GO5.0: the joint NERC–Met Office NEMO global ocean model for use in coupled and forced applications. Geoscience Model Development 7, 1069–1092. http://dx.doi.org/10.5194/gmd-7-1069-2014.

Meier, H.E.M., 2006. Baltic Sea climate in the late twenty-first century: dynamical downscaling approach using two global models and two emission scenarios. Climate Dynamics 27, 39–68. http://dx.doi.org/10.1007/s00382-006-0124-x.

Nakicenovic, N., Alcamo, J., Davis, G., de Vries, B., Fenhann, J., Gaffin, S., Gregory, K., Grubler, A., Jung, T., Kram, T., La Rovere, E., Michaelis, L., Mori, S., Morita, T., Pepper, W., Pitcher, H. M., Price, L., Riahi, K., Roehrl, A., Rogner, H.-H., Sankovski, A., Schlesinger, M., Shukla, P., Smith, S. J., Swart, R., van Rooijen, S., Victor, N., Dadi, Z., 2000. Special Report on Emissions Scenarios: A Special Report of Working Group III of the Intergovernmental Panel on Climate Change. IPCC.

Oki, T., Nishimura, T., Dirmeyer, P., 1999. Assessment of annual runoff from land surface models using Total Runoff Integrating Pathways (TRIP). Journal of the Meteorological Society of Japan 77 (1B), 235–255.

Oki, T., Sud, U.C., 1998. Design of Total Runoff Integrating Pathways (TRIP) – a global river channel network. Earth Interactions 2 (1), 1–36.

Olbert, A.I., Dabrowski, T., Nash, S., Hartnett, M., 2012. Regional modelling of the 21st century climate changes in the Irish Sea. Continental Shelf Research 41, 48–60. http://dx.doi.org/10.1016/j.csr.2012.04.003.

Pinnegar, J., Watt, T., Kennedy, K., 2012. Climate Change Risk Assessment for the Marine and Fisheries Sector, Defra.

Pope, V.D., Gallani, P.R., Rowntree, P.R., Stratton, R.A., 2000. The impact of new physical parametrizations in the Hadley Centre climate model: HadAM3. Climate Dynamics 16 (2–3), 123–146. http://dx.doi.org/10.1007/s003820050009.

Roberts-Jones, J., Fieldler, E., Martin, M.J., 2012. Daily, global, high-resolution SST and sea ice reanalysis for 1985–2007 using the OSTIA system. Journal of Climate 25 (18), 6215–6232. http://dx.doi.org/10.1175/JCLI-D-11-00648.1.

Schrum, C., Hübner, U., Jacob, D., Podzun, R., 2003. A coupled atmosphere/ice/ocean model for the North Sea and Baltic Sea. Climate Dynamics 21 (2), 131–151.

Sexton, D.M.H., Richardson, K., Harris, G., Karmalkar, A., Murphy, J., Brown, S., Tinker, J., 2013. (a) Potential Updates to Enhance the Utility of UKCP09; (b) Assessment of UKCP09, including Comparison against IPCC CMIP5 Multi-Model Simulations. Met Office Hadley Centre, Exeter, p. E4.

Sexton, D.M.H., Harris, G., Murphy, J., 2010. UKCP09: Spatially Coherent Projections. UKCP09 Additional Report. Met Office Hadley Centre, Exeter, UK.

Simpson, J.H., Bowers, D., 1981. Models of stratification and frontal movement in shelf seas. Deep Sea Research Part A. Oceanographic Research Papers 28 (7), 727–738.

Sutton, R., Dong, B., 2012. Atlantic Ocean influence on a shift in European climate in the 1990s. Nature Geoscience 5 (10), 1–5. http://dx.doi.org/10.1038/NGEO1595.

Tinker, J., Lowe, J., Holt, J., Pardaens, A., Wiltshire, A., 2015. Validation of an ensemble modelling system for climate projections for the northwest European shelf seas. Progress in Oceanography 138 (Part A), 211–237. http://dx.doi.org/10.1016/j.pocean.2015.07.002.

Wakelin, S.L., Holt, J.T., Proctor, R., 2009. The influence of initial conditions and open boundary conditions on shelf circulation in a 3D ocean-shelf model of the North East Atlantic. Ocean Dynamics 59 (1), 67–81. http://dx.doi.org/10.1007/s10236-008-0164-3.

Williams, K.D., Harris, C.M., Bodas-Salcedo, A., Camp, J., Comer, R.E., Copsey, D., Fereday, D., Graham, T., Hill, R., Hinton, T., Hyder, P., Ineson, S., Masato, G., Milton, S.F., Roberts, M.J., Rowell, D.P., Sanchez, C., Shelly, A., Sinha, B., Walters, D.N., West, A., Woollings, T., Xavier, P.K., 2015. The Met Office Global Coupled model 2.0 (GC2) configuration. Geoscience Model Development 8, 1509–1524. http://dx.doi.org/10.5194/gmd-8-1509-2015.